

1
2
3
4 **Drilling Constraints on Lithospheric Accretion and Evolution at Atlantis Massif,**
5 **Mid-Atlantic Ridge 30°N**
6
7
8

9 D.K. Blackman¹, B. Ildefonse², B.E. John³, Y. Ohara⁴, D.J. Miller⁵, and IODP
10 304-305 Science Party: N. Abe, M. Abratis, E.S. Andal, M. Andreani, S. Awaji, J.S.
11 Beard, D. Brunelli, A.B. Charney, D.M. Christie, J. Collins, A.G. Delacour, H.
12 Delius, M. Drouin, F. Einaudi, J. Escartín, B.R. Frost, G. Früh-Green, P.B. Fryer,
13 J.S. Gee, M. Godard, C.B. Grimes, A. Halfpenny, H-E. Hansen, A.C. Harris, A.
14 Tamura, N.W. Hayman, E. Hellebrand, T. Hirose, J.G. Hirth, S. Ishimaru, K.T.M.
15 Johnson, G.D. Karner, M. Linek, C.J. MacLeod, J. Maeda, O.U. Mason, A.M.
16 McCaig, K. Michibayashi, A. Morris, T. Nakagawa, T. Nozaka, M. Rosner, R.C.
17 Searle, G. Suhr, M. Tominaga, A. von der Handt, T. Yamasaki, X. Zhao
18
19

20 ¹ *Scripps Institution of Oceanography, UCSD La Jolla CA USA*

21 ² *Laboratoire de Tectonophysique Université Montpellier II, France*
22

23 ³ *Dept. Geology and Geophysics, University Wyoming, Laramie WY, USA*

24 ⁴ *Ocean Research Lab, Hydrographic & Oceanographic Dept, Tokyo, Japan*
25

26 ⁵ *Integrated Ocean Drilling Program, Texas A&M University, College Station TX, USA*
27
28
29

Abstract.

Expeditions 304 and 305 of the Integrated Ocean Drilling Program cored and logged a 1.4 km section of the domal core of Atlantis Massif. Post-drilling research results summarized here constrain the structure and lithology of the Central Dome of this oceanic core complex. The dominantly gabbroic sequence recovered contrasts with pre-drilling predictions; application of the ground truth in subsequent geophysical processing has produced self-consistent models for the Central Dome. The presence of many thin inter-fingered petrologic units indicates that the intrusions forming the domal core were emplaced over a minimum of 100-220 kyr, and not as a single magma pulse. Isotopic and mineralogical alteration is intense in the upper 100 m but decreases in intensity with depth. Below 800 m, alteration is restricted to narrow zones surrounding faults, veins, igneous contacts, and to an interval of locally intense serpentinization in olivine-rich troctolite. Hydration of the lithosphere occurred over the complete range of temperature conditions from granulite to zeolite facies, but was predominantly in the amphibolite and greenschist range. Deformation of the sequence was remarkably localized, despite paleomagnetic indications that the dome has undergone at least 45° rotation, presumably during unroofing via detachment faulting. Both the deformation pattern and the lithology contrast with what is known from seafloor studies on the adjacent Southern Ridge of the massif. There, the detachment capping the domal core deformed a 100 m thick zone and serpentinized peridotite comprises ~70% of recovered samples. We develop a working model of the evolution of Atlantis Massif over the past 2 Myr, outlining several stages that could explain the observed similarities and differences between the Central Dome and the Southern Ridge.

1. Introduction

1 Deep drilling of the domal core of Atlantis Massif, Mid-Atlantic Ridge 30°N (Figure 1),
2 has provided insights into the formation of slow-spread lithosphere, and constraints on
3 the structure and evolution of Oceanic Core Complexes (OCC) that could not have been
4 obtained from seafloor mapping and sampling alone. The information obtained by coring
5 and borehole logging were a key motivation for increasing the sophistication of regional
6 geophysical analyses, which, in turn, advanced interpretations of the subsurface structure.
7 Integrated Ocean Drilling Program (IODP) Expeditions 304-305 drilling results
8 (Blackman *et al.*, 2006) provided first-order information that the Central Dome is
9 composed of dominantly gabbroic rocks, in contrast to early geological and geophysical
10 interpretation that predicted this region to be underlain by ultramafic rocks. Post-
11 expedition investigations have targeted a variety of more complex questions. In this paper
12 we summarize many of the post-cruise results and compare these to results from seafloor
13 studies on the southern part of the domal core, the Southern Ridge (Figure 1a). We
14 proceed with new analyses, discussing the implications in terms of the formation and
15 evolution of the whole core complex.

16
17 Slow-spread ocean lithosphere accretes and evolves via temporally and spatially variable
18 magmatic and tectonic processes (e.g., Bonatti and Honnorez, 1976; OTTER, 1984; Dick,
19 1989; Lin *et al.*, 1990, Sinton and Detrick, 1992; Cannat, 1993, Lagabrielle *et al.*, 1998).
20 OCC, in particular, mark significant periods (1-2 Myr) where a distinct mode of rifting/
21 accretion persists, in contrast to the more typical interplay between magma supply and
22 faulting that generates the ubiquitous abyssal hills. Long-lived displacement along
23 detachments active within the ~20 km wide axial zone of a spreading center exhume the
24 characteristic domal cores of an OCC, often capped by spreading-parallel corrugations
25 (e.g., Cann *et al.*, 1997; Tucholke *et al.*, 1998). Beneath this exposed fault zone, gabbroic
26 rocks with lenses, and possibly more significant volumes of mantle peridotite are present,
27 providing access to a major component of Earth's deep lithosphere for detailed chemical
28 and physical property investigations. Conditions of OCC development are documented
29

1 by igneous and metamorphic assemblages, as well as by deformation recorded during
2 evolution of the footwall.

3
4 Atlantis Massif is a young OCC where contextual data from regional geophysical
5 surveys, as well as seafloor mapping and sampling is good, and major structural blocks
6 within the faulted lithosphere have been identified (Figure 1). Drilling targeted the
7 Central Dome while a majority of the seafloor studies have taken advantage of outcrops
8 accessible on the steep face of the Southern Ridge, the ‘South Wall’ (Figure 2), where the
9 dome plunges toward the transform valley. In the final section of this paper, we consider
10 results for both of these parts of Atlantis Massif, and we develop a model for the
11 formation and evolution of the whole OCC.

12
13 Some initial inferences based on pre-drilling and/or shipboard analysis (Blackman *et al.*,
14 2006) have been superseded by new interpretations that incorporate in-depth post-cruise
15 results, as discussed in the following sections. These updates include: consistency of
16 geophysical models of the Central Dome of Atlantis Massif; the age of crust drilled (and
17 associated plate spreading rate during core complex formation); the genesis of recovered
18 olivine-rich troctolite; the nature of metamorphism; and systematic tectonic rotation of
19 the footwall based on paleomagnetic data.

21 **2. Geologic Setting**

22 Sea surface magnetic anomalies indicate that the lithosphere comprising Atlantis Massif
23 is between 0.5 and 2 Ma. Average plate spreading rate over the past ~5 m.y. has been ~24
24 mm/yr (full rate, Pariso *et al.*, 1996). Atlantis Massif was initially hypothesized to be an
25 OCC on the basis of morphologic and backscatter mapping, and dredging results that
26 documented the shallow, corrugated and striated domal core underlain by mafic and
27 ultramafic rocks (Cann *et al.*, 1997). The spreading-parallel corrugations are equated with
28 similar-scale features mapped on continental detachment faults (John, 1987), and suggest
29 it was a slip surface associated with the detachment fault that unroofed the dome.

1 Schroeder and John, (2004) and Karson *et al.* (2006) document deformation within a
2 zone that confirms the existence of a long-lived normal fault at the top of at least parts of
3 the Southern Ridge. The juxtaposition of volcanic eastern blocks against the corrugated
4 dome, where southern ridge samples include gabbroic rocks and serpentinitized peridotite,
5 supports the OCC model (Figure 2). Gravity and seismic data indicate that significant
6 portions of the footwall to the detachment contain rocks with anomalously high density
7 (200-400 kg/m³ greater than surrounding rock; Blackman *et al.*, 1998; Noonan *et al.*,
8 2003), and velocities (4-6 km/s in the upper km, compared to average Atlantic upper crust
9 at ~3-5 km/s; Canales *et al.*, 2008, Collins *et al.*, 2009).

10
11 The development of this OCC at the eastern intersection of the Mid-Atlantic Ridge
12 (MAR) with the Atlantis fracture zone is just one of three instances over the past ~9 m.y.
13 where an OCC is inferred to have formed at one of the inside corners in this area (Cann *et al.*, 1997). Both the older OCCs shoal to 1000 m, somewhat deeper than the peak of
14 Atlantis Massif (Blackman *et al.*, 1998; 2002) but similar to the average depth of the
15 Southern Ridge (Figure 1b). The active serpentinite-hosted Lost City hydrothermal vent
16 field (Kelley *et al.*, 2001; Früh-Green *et al.*, 2003) is located just below the peak of the
17 massif, the apex of the Southern Ridge. The Central Dome extending smoothly to the
18 north is several hundred meters deeper, and it is against only this part of the footwall that
19 the juxtaposed volcanic hanging wall exists. It is assumed to overlie the detachment where
20 it extends at depth. The existence of large-throw normal faults toward the median valley
21 likely indicates that major slip along the detachment has ceased (e.g., Cannat *et al.*,
22 2009).

23
24
25 Mapping and sampling along the southern ridge of Atlantis Massif (Figure 2) shows that
26 detachment processes in that area were concentrated in a zone about 100 m thick
27 (Schroeder and John, 2004) and that the fault is continuous for at least a few km in the
28 spreading direction (Karson *et al.*, 2006). Thin carbonate sediment in many places is
29 lithified and covers much of the detachment on top of the domal core, impeding direct

mapping and sampling of fault surface (Blackman *et al.*, 2002). Below the carbonate interval, less than 1 m thick, a breccia unit 1-3 m thick has been mapped locally, unconformably overlying the detachment shear zone (Karson *et al.*, 2006). Basaltic rubble was mapped and sampled along a transect across the Central Dome, and the alteration minerals in these samples (chlorite, amphibole and later clays) indicate metamorphism at temperatures too high for near-seafloor conditions. Blackman *et al.* (2002) inferred this to indicate they are probably remnants from the base of the hanging wall after its displacement along the detachment fault. Additional aspects of the Southern Ridge geology and geophysics are discussed in Section 7; we focus the next several sections on the drilling results for the Central Dome.

3. Drilling Strategy and Gabbroic Sequence Recovery

Determining the processes that operate during formation of OCCs was the overriding goal of drilling at Atlantis Massif (Blackman *et al.*, 2004). In addition, the potential for recovery of unaltered ultramafic rock, suggested to be present at depths as shallow as several hundred meters sub-seafloor based on initial seismic analyses (Canales *et al.*, 2004; Collins *et al.*, 2003), generated significant interest in the community. The drilling plan for IODP Expeditions 304 and 305 was designed to address questions about the proposed detachment zone itself, the footwall, and geochemical and structural relationships between the domal core and the volcanic hanging wall (Table 1, Blackman *et al.*, 2004).

Table 1. Hypotheses targeted by IODP Expeditions 304 & 305.

1. A major detachment fault system controlled the evolution of Atlantis Massif.
2. Plate flexure (rolling hinge model) was the dominant mechanism of footwall uplift.
3. Significant unroofing occurred during formation of this OCC.
4. The nature of melting &/or magma supply contributed to episodes of long-lived lithospheric faulting.
5. Expansion associated with serpentinization contributed significantly to uplift of the domal core.
6. The Mohorovicic discontinuity (Moho) at Atlantis Massif is a hydration front.
7. Positive gravity anomalies at Atlantis Massif indicate relatively fresh peridotite.

1
2 Attempts to start a re-entry hole in the western part of the hanging wall (IODP Sites
3 U1310 and U1311; Figure 2) were unsuccessful; no samples were obtained from an
4 unexposed section of the detachment, hypothesized to underlie this block (Canales *et al.*,
5 2004). Minimal recovery from the upper ~10 m of the hanging wall obtained relatively
6 fresh basalt, but the samples are insufficient for detailed structural or petrologic studies.
7

8
9 In contrast, drilling conditions on the Central Dome at IODP Site U1309 (Figure 2) were
10 excellent. A pilot hole (U1309B) was drilled to bit destruction, core was recovered
11 throughout the 101 m deep section, and the hole logged. Following an aborted attempt to
12 establish a re-entry hole (U1309C), Hole U1309D was established 20 m to the north of
13 Hole U1309B and penetrated to 1415 mbsf, over a series of alternating coring and
14 logging runs. A combination of instrument problems and poor weather precluded the final
15 seismic logging run. Therefore, only the upper 800 m of the formation have this
16 coverage, but other borehole measurements were obtained throughout the >1400m hole.
17 The hole was in good condition at the end of Expedition 305 and our expectation is that it
18 remains open and could be re-entered should future logging, monitoring, or drilling
19 efforts be pursued.

20
21 The location of Holes U1309B and D reflected a variety of factors. The smoothness and
22 scale of the domal core were inferred to indicate homogeneous properties (composition,
23 deformation, alteration) over large areas; supporting this inference were the continuity
24 and pervasiveness of a strong seismic reflection 0.2-0.5 s two-way travel time beneath the
25 seafloor, underlying both the Southern Ridge and the Central Dome (Canales *et al.*,
26 2004). The drill site was thus selected avoiding fields of rubble known to be present on
27 the dome (Blackman *et al.*, 2002). Based on pre-existing seafloor mapping data showing
28 a rubble-free zone near (~400 m), but not exactly on, multi-channel seismic profiles, Site
29 U1309 was located in the southern Central Dome. The site is at the southern end of the

1 eastern Near-Ocean-Bottom-Explosive-Launcher (NOBEL) refraction line (Figure 2) and
2 along a longer, traditional refraction line.

3
4 The ~1.4 km sequence recovered at Site U1309 was dominantly gabbroic, only a few
5 percent of the drill core consisted of ultramafic rock (Blackman *et al.*, 2006). Recovery
6 was high, averaging ~75% below the uppermost few tens of meters that were either cased
7 (Hole U1309D) or typical low return for the initiation of a deep hole in hard rock (Hole
8 U1309B). The high recovery and subsequent integration of borehole logs with the cores
9 indicate that these samples adequately represent the in-situ section. The thick mafic
10 section recovered was key in shifting the original paradigm that detachment faulting and
11 OCC development occur because a portion of the spreading center rifts without
12 significant magmatic input (e.g., Karson, 1990, Tucholke and Lin, 1994). Drill and
13 dredge data from other corrugated core complexes (Dick and others, 2000, MacLeod *et*
14 *al.*, 2002, Escartín *et al.*, 2003; Kelemen *et al.*, 2007), together with work at the
15 (uncorrugated, but likely detachment-controlled) Kane inside corner high (Karson *et al.*,
16 1997), had already indicated that there was magmatic activity during OCC development,
17 but the volume percent was often (although not always, Karson, 1987) considered to be
18 low. Three recent models propose that an increase in local magmatism plays an important
19 role in the development of core complexes and that OCCs do not represent the magma-
20 starved end-member of slow-spreading ridges. Ildefonse *et al.* (2007a) suggest that
21 increased local magmatism plays a role in establishment of long-lived detachment
22 faulting. Tucholke *et al.* (2008) use numerical models to predict that increased axial
23 magmatism triggers a shift in faulting away from the active detachment, thus ending
24 OCC development. MacLeod *et al.* (2009) propose that a final stage in the cycle of OCC
25 formation is along-strike propagation of a magmatically robust axial volcanic ridge,
26 which cuts through the detachment, relieves stress and thus ends the long-term activity of
27 the fault.

1 A secondary goal during Expedition 304 was to obtain samples of the uppermost few
2 meters of the corrugated dome, with the aim of sampling fault rock from the principal slip
3 surface and damage zone associated with the inferred detachment at the seafloor. The
4 *JOIDES Resolution*, with the drill tools onboard at the time, was understood to be less
5 than ideal, but both the principal slip surface and overlying sediment were valuable, so
6 effort was expended for this task on Expedition 304, after progress in Hole U1309D
7 exceeded expectations. This series of shallow holes U1309A, and E-H ranged from 1-4 m
8 penetration below seafloor. Recovery of basement rock was less than a few percent of the
9 apparent cored interval. Drilling-disrupted fossiliferous ooze (0-2.5 m) was recovered at
10 Holes U1309A, E, F and G. Holes U1309F, G, and H also included fragments of
11 metabasalt, hyaloclastite, fractured diabase or fragments of talc schist inferred to be fault
12 rock. Similar chromite-bearing talc-tremolite-chlorite schist fragments were found in the
13 uppermost part of the deeper holes, as a clast in a fault breccia at 20 mbsf in Hole 1309B,
14 and as a 10 cm cored interval at 23 mbsf in Hole 1309D. The same assemblages are
15 found in veins replacing ultramafic horizons in the upper 300 m of the core. These rock
16 types are identical to samples obtained within well-mapped seafloor detachment shear
17 zones (15°45'N MAR, MacLeod *et al.*, 2002, and Escartín *et al.*, 2003; the Southern
18 Ridge of Atlantis Massif, Boschi *et al.*, 2006), but are absent in the rest of the recovered
19 sequence at Site U1309. Thus, it is likely that they represent samples from a detachment
20 fault, but our recovery falls short of providing irrefutable evidence for (or against) a
21 major shear zone at the seafloor on the Central Dome. The upper 80 m of Holes 1309B
22 and D contain fault breccias composed of basaltic clasts with a green amphibole-rich
23 matrix, and zones of intensely fractured gabbro. They are cut by undeformed but strongly
24 altered basalt and diabase intrusions which comprise about 40% of the recovered core in
25 this interval (Blackman *et al.*, 2006). These fault breccias and fractured gabbros may be
26 the expression within the gabbro of the well-developed shear zone in serpentinite
27 described from the Southern Ridge of the massif (Karson *et al.*, 2006).
28
29

4. Incorporation of the New Constraints in Revised Geophysical Analyses

This section reconciles recovery of a dominantly gabbroic sequence with the pre-drilling predictions that the dome was underlain mostly by ultramafic rocks, with the potential for fresh peridotite at a shallow depth. Several factors led to initial preference for a model where Atlantis Massif had a core that was dominantly ultramafic. Mapping along the south wall, thought to provide a cross-section through the domal core, produced a high percentage of serpentinized mantle peridotite samples (~70%); gabbro makes up a majority of the remaining sample suite (Blackman *et al.*, 2002, Boschi *et al.*, 2006). Second, a tomographic inversion fit the NOBEL data well when the top of a >7.5 km/s layer was modeled at 600 mbsf (Figure 3a-b; Collins *et al.*, 2003). This shallow, sharp transition to high velocity was consistent with interpretation of the multi-channel seismic (MCS) reflection results, where a strong, isolated, continuous reflection arose from an impedance contrast at around this depth throughout the domal core (Canales *et al.*, 2004). Since velocities of 7.6 km/s and higher would indicate little-altered, olivine rich rock typical of mantle peridotite (e.g. Minshull *et al.*, 1998), Collins *et al.* (2003) concluded that Moho could be extremely shallow (< 1 km) locally within the dome. Third, gravity anomalies indicated that the core of Atlantis Massif has a density that is, on average, 200-400 kg/m³ higher than the adjacent tectonic blocks (Blackman *et al.*, 1998, Nooner *et al.*, 2003). Juxtaposition of average crust (2850 kg/m³) against a mix of altered and fresh peridotite (~3300 kg/m³) with lesser gabbro could produce this relative density signature. The processing of the regional gravity and seismic data prior to 2004 used standard marine techniques. For gravity, this included the assumption that the density contrast at the seafloor was constant throughout the region (Blackman *et al.*, 1998; 2002). For the seismic refraction analysis, a presumption of dominant vertical gradients, as opposed to horizontal velocity contrasts, underlay the modeling approach (Collins *et al.*, 2003). For the MCS processing, a strong mute (Canales *et al.*, 2004) eliminated deeper, more variable reflectivity, which was later shown to occur by Singh *et al.* (2004).

1 With the geological information available from Site U1309, subsequent geophysical
2 analyses considered additional complexity. This analysis resulted in a model of the
3 Central Dome consistent with all available constraints, including borehole lithology,
4 gravity, and seismic velocity. The post-drilling gravity modeling takes into account the 3-
5 D structure of the hanging wall and domal core at Atlantis Massif (Figure 1c; Blackman
6 *et al.*, 2008). The positive 30-40 mGal residual gravity anomaly can be explained if the
7 core is gabbroic with density of 2900 kg/m³, the adjacent basaltic block is significantly
8 fractured with average density 2600 kg/m³, and the portion of the lithosphere deeper than
9 1.5 km mbsf that has density lower than mantle rock (either dominantly gabbroic,
10 peridotite that is significantly altered, or a mix thereof) is ~3 km thick within the domal
11 core.

12
13 Post-drilling seafloor refraction modeling showed that shallow mantle velocities,
14 although permissive based on the NOBEL data, are not required (Collins *et al.*, 2009;
15 Figure 3c); velocities in the upper several hundred meters of the new model are typical of
16 mafic rock (≤ 6.5 km/s). Tomographic inversion of refracted arrivals recorded by the 6-
17 km MCS streamer (Canales *et al.*, 2008) obtained a similar velocity structure to 1.0-1.5
18 km depth along Lines 10 and 4 (the latter model shown in Figure 3d) where they cross
19 the Central Dome (Figure 2). More detailed analysis of the upper few hundred meters is
20 possible when the MCS refraction data are downward continued, which, in turn, allows
21 greater accuracy of structure determined for the 0.5-1.5 km deep section. Arrival-time
22 tomography using downward-continued data for a portion of Line 10 (Harding *et al.*,
23 2007) confirmed that velocities in the upper 1.5 km of the footwall are 6.5 km/s and
24 lower. The velocity-depth curve for the revised NOBEL model (Collins *et al.*, 2009)
25 brackets the sonic log data for Hole U1309D. A recent MCS tomographic result for Line
26 10 (Blackman *et al.*, 2009; Figure 4), 1.8 km to the north of the hole, is similar although
27 velocities are somewhat lower in the interval between 150-550 mbsf. Analysis of a 40-km
28 long airgun refraction profile across the Central Dome (approximately along MCS Line
29 10, Figure 2) subsequently provided coarser constraints on velocities to depths as great as

1 7 km. Travel-time tomography (Blackman and Collins, 2010) indicated that significant
2 volumes of rock with mantle-like velocity (>7.5 km/s) occur only below ~ 5 km
3 subseafloor depth within the dome (grading downward within the coverage to 7.8 km/s),
4 and are more than 6 km deep in the axial valley.

5
6 We cannot yet confirm the source(s) of the impedance contrast that gives rise to the
7 strong reflection imaged throughout much of the dome (the 'D reflector', Canales *et al.*,
8 2004). Reflectivity modeling based on borehole velocity and density logs (Collins *et al.*,
9 2009) does produce an arrival from an impedance contrast near an alteration boundary
10 observed in the recovered core from 380 m subseafloor depth in Hole U1309D (Figure
11 4d). However, the amplitude of this predicted reflection is modest. A more likely
12 candidate for the D reflector may be the base of a thin (~ 100 m), low velocity layer
13 (~ 3 - 3.5 km/s) immediately below the seafloor. Collins *et al.* (2009) showed that such a
14 layer overlies ~ 5.5 km/s material (Figure 3). This interpretation is similar to one put
15 forward for OCCs in the Philippine Sea (Ohara *et al.*, 2007). However, complexity due to
16 seafloor scattering in the published reflection image near Site U1309 (Collins *et al.*,
17 2009), and the offset between Hole U1309D and the closest MCS line (Line 4, ~ 400 m
18 away) preclude our ability to make a detailed correlation between local rock properties
19 and any given reflector.

20
21 Prior to Expedition 304/305, geophysical and geological studies supported the hypothesis
22 that a significant fraction of the subseafloor at Atlantis Massif was ultramafic. In
23 retrospect, the discovery that virtually everything recovered by drilling was mafic
24 suggests that a more comprehensive exploration of alternative structural/lithologic
25 distributions may have resulted in a more complex suite of hypotheses to be tested and
26 could have had an impact on the design of the experiment (drill site selection, borehole
27 experiments, or additional mapping). The surprise and disappointment when mantle was
28 not encountered during Expedition 305 was strongest in the non-geophysical
29 communities, who are generally less aware of the inherent non-uniqueness in most

1 geophysical analyses. However, the geophysical community can also benefit from the
2 experience, if the tendency to rush exciting initial findings to press in a form that does not
3 clearly portray the realm of uncertainties and unknowns can be tempered. This means
4 detailing limits due to both the data and coverage themselves and any assumptions that
5 underlie the processing steps. Whereas the original proposal PIs emphasized OCC
6 structure and evolution in their drilling request and this remained the stated main
7 emphasis for drilling (Table 1; Blackman et al., 2004), the broader community's interest
8 was probably more strongly captured by the prospect of sampling fresh mantle. Future
9 endeavors where the latter is the target will probably benefit from detailed geophysical
10 analysis and critical review, in light of a range of possible models and hypothesis tests,
11 before finalizing the project plan. However, since the purpose of drilling is to obtain
12 information unattainable in any other way, post-drilling re-evaluation of regional data
13 will almost always occur, bringing additional insights on the core and logging
14 discoveries.

15 **5. Summary of Drilling Results**

16 The core and borehole data obtained at Site U1309 contain a wealth of information on the
17 accretion and initial evolution of oceanic lithosphere. Analyses are ongoing and expected
18 to continue for many years. In this section, we provide a summary of post-drilling results
19 to date since the individual studies have been published outside the traditional
20 geophysical literature and each focused on only an aspect of the recovered section. While
21 more detail is available in the original papers, this summary provides a basis for
22 considering the implications discussed in subsequent Sections. We focus on how results
23 thus far inform two aspects of Atlantis Massif's development— magmatic accretion and
24 deformation within ~15 km of the axis of spreading. Some of these results may point to
25 processes specific to periods when OCC develop, several are likely applicable to slow-
26 spread ocean lithosphere in general.
27
28
29

5a. New Information on Magmatic Accretion

The uppermost rock types recovered at Site U1309 include diabase and/or basalt that comprise 35-40% of recovered core above 120 mbsf (Figures 4a-b), and that are the sole type recovered from the top ~30 m. These intrusive rocks are little deformed but strongly amphibolitized. They show clear chilled margins against cataclastic gabbro and amphibole-rich fault breccias dominated by metabasaltic clasts, as well as against undeformed diabase. Correlation between Holes U1309B and D suggests that they form sill-like bodies 5-10 m thick dipping at about 30° (Section 5c), an inference supported by preferred alignment of phenocrysts dipping 10°-40° in diabase at 85-100 mbsf. A few steep contacts were recovered from Hole U1309B. McCaig *et al.* (2010) suggested that the latter intrusions occurred subparallel to a steeply-dipping fault zone (that later rotated, Section 5b). Other intervals of diabase were sampled throughout the sequence but, below 120 mbsf, they are sparse and their (recovered) thickness rarely exceeds one meter (Figure 4a-c; Blackman *et al.*, 2006). The composition of all diabase recovered falls within the range of basalt compositions for the MAR 30°N axial region (Godard *et al.*, 2009).

The dominantly gabbroic sequence underlying the upper diabase units comprises hundreds of individual lithologic units ranging in composition from gabbro, to oxide-, olivine- and troctolitic gabbro, troctolite, and olivine-rich troctolite. Each igneous unit was identified during shipboard characterization on the basis of modal composition (Figure 5a) and/or grain size changes downcore. Contacts between units were recovered in many instances (Figure 5c,d), allowing recognition of relative age. Based on these contact relations, the scale of intrusion varies from centimeters to tens of meters, with the latter thickness being most common (John *et al.*, 2009). In general, relatively evolved rock types intrude more primitive rock types although the inverse sense of intrusion is also observed locally (Blackman *et al.*, 2006; John *et al.*, 2009).

1 Leucocratic intrusions (cm-scale thickness) cut the sequence and, together with oxide
2 gabbro intervals, host zircon grains that have been used to obtain crystallization ages of
3 the recovered crustal section. Grimes *et al.* (2008) used an ion microprobe (SIMS)
4 method and $^{206}\text{Pb}/^{238}\text{U}$ ratios to determine a weighted mean age for the recovered
5 sequence of 1.20 ± 0.03 Ma (Grimes *et al.*, 2008), from which they propose that accretion
6 occurred over a minimum of 100-200 kyr.

7
8 Modal mineralogy and bulk rock geochemistry (e.g. Figures 5a and 5b) of the gabbroic
9 sequence are typical of a cumulate series crystallizing from a mid-ocean ridge basalt
10 (MORB) source. Observed co-variations in plagioclase and clinopyroxene composition
11 between olivine gabbro and gabbro are also typical. However, Godard *et al.* (2009)
12 determined that the bulk composition of Hole U1309D does not represent the
13 complement to basalts recently erupted at the nearby spreading axis. On the basis of
14 higher than expected trace element and Fe contents, these authors concluded that a
15 significant amount of evolved melt was trapped and crystallized within the sequence.
16 Plagioclase + liquid thermometry yielded a crystallization temperature of $1230 \pm 25^\circ\text{C}$ for
17 the troctolite and gabbro (Drouin *et al.*, 2009). Low-pressure crystallization depths (≤ 200
18 MPa, ~ 6 km) were inferred based on the modal relationships and chemistry of cumulus
19 and inter-cumulus phases (Suhr *et al.*, 2008, Godard *et al.*, 2009). Godard *et al.* (2009)
20 noted the complexity of modal composition for the many thin igneous units, and the
21 variability of contact type, ranging from sharp to diffuse, in their preference for a model
22 where the sequence was built by multiple injections of melt. In contrast, Suhr *et al.*
23 (2008) prefer a model where a small number of several-hundred-meter-thick magma
24 bodies each differentiates over a finite period, to provide evolved melts that react with
25 host rock and intrude earlier-crystallized intervals.

26
27 Suhr *et al.* (2008) interpreted a repeating pattern of olivine gabbro grading upward into a
28 mainly gabbro to gabbronorite interval which, in turn, is overlain by a thin oxide gabbro
29 interval (Figure 6a). Mg# ($\text{Mg}/\text{Mg}+\text{Fe}$) and trace element contents (Godard *et al.*, 2009)

1 support the idea that a staggered sequence of a few magmatic pulses built the recovered
2 section. Decreases in bulk rock Mg# at 640 mbsf and 1235 mbsf coincide with increases
3 in Yb content (Figure 6b-c), suggesting that these mark possible boundaries of different
4 magmatic units. Suhr *et al.* (2008) prefer to locate the top of the central magmatic body
5 around 800 mbsf, below the fault zone at 750 mbsf, but their analysis did not include the
6 sequence above this fault. The choice of ~640 mbsf as the boundary is similar but not an
7 exact match to a jump in Pb/U zircon ages for Fe-Ti oxide gabbro samples from $1.17 \pm$
8 0.02 Ma at 579 mbsf to 1.24 ± 0.02 Ma at 623 mbsf (Grimes *et al.*, 2008; Figure 6d).
9 Regardless, while repetition of a few 100's-m-thick intrusions and subsequent self-
10 intrusion during a simple MORB crystallization sequence addresses some of the
11 lithologic variation in the hole, it cannot by itself account for the olivine-rich troctolite
12 intervals.

13
14 Olivine-rich troctolite (>70% olivine with low modal plagioclase and clinopyroxene) is
15 present as relatively thin (~1 to 12 m) units within two main intervals (~310-350 mbsf
16 and 1090-1235 mbsf, Figure 6a). Bulk rock geochemical signatures of these troctolites
17 are more primitive than other mafic samples from the ocean crust (Godard *et al.*, 2009;
18 Figure 5b). Cumulate textures are observed in the olivine-rich troctolites (Blackman *et*
19 *al.*, 2006; Figure 7), but several lines of evidence suggest that these rocks are not simply
20 the first-crystallized product of a closed, fractionating magma body. Based on mineral
21 chemistry and textural relations, Drouin *et al.* (2009, 2010) support a model whereby the
22 olivine-rich troctolites formed through open-system reaction between initial olivine-
23 bearing rocks and later MORB melts. Trace element patterns for melts in equilibrium
24 with the measured in-situ plagioclase, clinopyroxene and olivine compositions (Figure
25 7a) illustrate that the olivine is in complete disequilibrium with MORB melts that
26 crystallized the plagioclase and clinopyroxene (Drouin *et al.*, 2009). Whereas modest
27 intra-crystalline deformation of olivine grains is observed, surrounding oikocrystic
28 clinopyroxene and plagioclase crystals are undeformed (Figure 7b-c), indicating that
29 crystallization of the impregnating melt occurred either rapidly or under static conditions.

1 The chemistry of the core of clinopyroxene grains differs from their rim in the olivine-
2 rich troctolite units (Suhr *et al.*, 2008, Drouin *et al.*, 2007; 2009). Ti is enriched and Al
3 and Cr are depleted toward the rim, whereas plagioclase and olivine grains are unzoned.
4 Using geochemical constraints Suhr *et al.* (2008) estimated melt:rock ratios around 3:1,
5 with the original host rock being mantle peridotite. Drouin *et al.* (2009) also concluded
6 that high melt:rock ratios characterized the olivine-rich troctolite intervals.

7
8 A variety of observations, therefore, demonstrate that the olivine-rich troctolites were
9 produced by infiltration and assimilation of olivine-rich rock by a MORB melt. These are
10 consistent with, but do not prove that the pre-existing olivine grains were derived from
11 mantle peridotite. Drouin *et al.* (2010) interpreted the observed relatively stronger
12 concentrations of olivine [001] preferred orientation in some of these rocks to result from
13 dunitization and disaggregation of mantle peridotite which, if not heavily fluxed with
14 melt, would be expected to display flow-induced [100] preferred alignment in this setting.
15 Disruption of preexisting high-temperature crystallographic preferred orientations during
16 melt influx is also suggested by the common occurrence of adjacent grains with neighbor
17 crystallographic orientations. Suhr *et al.* (2008) also noted microstructural evidence in
18 their interpretation of the olivine-rich troctolites as having mantle peridotite origin. They
19 based their conclusion on the fine (0.5 mm) size, and common extinction of adjacent
20 olivine grains (Figure 7e) together with both observed and modeled Cr and Ni
21 geochemistry.

22
23 A few thin intervals of mantle peridotite showing lower melt:rock ratios (van der Handt
24 and Hellebrand, 2010) were recovered from Site U1309 (<0.5% of the total core; Figure
25 4), all from above 200 mbsf (Blackman *et al.*, 2006). Petrologic and geochemical analysis
26 of multiple samples from these intervals (Tamura *et al.*, 2008; Godard *et al.*, 2009) show
27 that three residual harzburgite screens or remnants remain (59, 155, and 174 mbsf) after
28 having been surrounded and impregnated by the gabbroic melt that form the Site U1309
29 sequence. Three other thin ultra-mafic intervals are most likely original cumulates

(wehrlite, dunite) also penetrated by MORB melts. Together with the results of detailed analyses on the olivine-rich troctolites, the picture that emerges is one where the lithospheric section sampled at the Central Dome of Atlantis Massif was formed piecemeal as a stack of gabbroic bodies intruded into mantle peridotite and earlier solidified gabbro. Associated with this stack are screens of peridotite and larger zones of olivine-rich troctolite that have formed by interaction with gabbroic melt.

5b. Lithospheric Deformation

In contrast to other sections of ocean lithosphere obtained by drilling at, or in the vicinity, of an OCC (see Section 6), the recovered sequence lacks pervasive deformation, either brittle or plastic (Blackman *et al.*, 2006). The zones where deformation intensity is 2 or higher (on a scale from 0 to 5, undeformed to ultramylonite/cataclasite) are narrow (cm-m scale, Figures 8 and 9) and sparse throughout the core. High strain processes associated with grain-size reduction were apparently confined to narrow intervals. We cannot rule out the occurrence of sub-meter scale, high-strain intervals that were not recovered in core (white portion of lithology columns in Figure 4), such as intervals 4-16 mbsf in Hole U1309B, 0-20 m and 103-117 mbsf in Hole U1309D. Apart from these intervals, there is no evidence for high strain zones that are several meters thick.

Cataclastic structures are more common in the upper part of the core (<750 mbsf) than in the lower part, and a number of thin cataclastic and breccias zones are cut by diabase intrusions in the upper 80 m of the core (Blackman *et al.*, 2006). Most of the crystal plastic deformation is recorded in the upper 310 m of the section, but the interval 640-700 mbsf and another centered on 1300 mbsf also show plastic deformational structures (Figure 8a). Fault gouge recovered from 750 mbsf has significantly higher intensity cataclastic deformation than any other interval (Figure 8b).

At Site U1309, fragments of talc-tremolite schist sampled only in the uppermost 25 meters (Blackman *et al.*, 2006) document intense deformation, with syntectonic growth

1 of phyllosilicates associated with metasomatism and fluid flow. If these represent, as we
2 suggest, an *in situ* talc-rich deformed zone it would have to be very narrow (≤ 25 mbsf)
3 based on drilling, coring, and recovery from all the holes at the Site (Figure 2).

4 Brecciation of fine-grained metadiabase at greenschist facies conditions occurred in
5 several intervals within the upper 130 m, but not greater depths. McCaig *et al.* (2010)
6 infer that these basaltic melts were intruded in close proximity to, if not within, a region
7 of faulting. They interpret high $^{87}\text{Sr}/^{86}\text{Sr}$ and low $\delta^{18}\text{O}$ in samples from the upper ~ 100 m
8 at Site U1309 to indicate high fluid flux within a detachment zone whose activity was
9 coeval with magmatism that produced diabase. This resulted in only highly localized
10 deformation, such as brecciation and the formation of talc-tremolite-chlorite schist. In a
11 later Section (7), we discuss differences between the deformation observed in the upper
12 ~ 100 m of the Central Dome and that determined to define a detachment shear zone atop
13 the Southern Ridge (Karson *et al.*, 2006).

14
15 Of the several narrow fault zones identified in core from Hole U1309D (dashed lines in
16 Figures 6, 8), the most significant fault is located $\sim 742\text{--}761$ mbsf (Michibayashi *et al.*,
17 2008; John *et al.*, 2009), where a continuous 80-cm sample of gouge was obtained,
18 although recovery was generally poor in the interval. Borehole logs (neutron porosity,
19 density, resistivity) suggest that the fault zone could be up to 5 m thick. Permeability of
20 the (ultra) cataclasite is 1-3 orders of magnitude greater than that of adjacent rock types,
21 although not unusual, at $10^{-17}\text{--}10^{-19}$ m², for intrusive mafic rock (Michibayashi *et al.*,
22 2008). The presence of amphibole together with a local drop in borehole resistivity
23 (Figure 4e) indicates hydration of the zone. Michibayashi *et al.* (2008) determined that
24 seams of aluminous actinolite and plagioclase indicate brittle failure at high temperature
25 (>600 °C). The relatively modest permeability is explained by subsequent sealing by
26 hydrous minerals that prevented further circulation and allowed preservation of water in
27 the crust.

1 Paleomagnetic data provide constraints on tectonic rotation experienced by the footwall
2 rocks. Remanent inclinations of core samples are approximately 10° shallower than
3 expected for reversely magnetized rock at the site, suggesting significant tectonic rotation
4 since acquisition of magnetic remanence. IODP cores in igneous rock are not azimuthally
5 oriented so magnetic declinations cannot ordinarily be determined. However, it has been
6 possible to independently reorient a number of core pieces by matching oriented borehole
7 features imaged with the Formation MicroScanner to features observed in core pieces.
8 Morris *et al.* (2009) report results for 34 samples from the upper 400 m of the section.
9 The mean full remanence vector from these oriented samples has a southwesterly
10 declination and indicates a minimum of $\sim 45^\circ$ counterclockwise rotation about a
11 horizontal axis oriented 011° (ridge axis parallel). Although shipboard measurements
12 imply that most core samples from the upper 180 m have magnetic inclinations close to
13 that expected, the reoriented data from this interval have declinations displaced to the
14 SW, thus rotation is required. Interpretation of inclination data from the 400-1415 mbsf
15 interval, and incorporation of directional constraints from local seafloor corrugations
16 (Garcés and Gee, 2007) yield an essentially identical amount of rotation. Using average
17 paleomagnetic inclinations alone, Zhao and Tominaga (2009) suggest rotation up to $\sim 50^\circ$.
18 These results demonstrate that the footwall experienced significant overall rotation since
19 acquisition of magnetization (i.e., below 550°C), consistent with flexural rotation during
20 exposure of the detachment at the seafloor. The magnitude of rotation recorded by the
21 paleomagnetic results from the Central Dome is comparable to what has been inferred
22 from seafloor morphology modeled as blocks back-tilted via slip along a detachment fault
23 (Smith *et al.*, 2008; Schouten *et al.*, 2010).

24
25 The large footwall rotation, certainly for the upper 400 mbsf (Morris *et al.*, 2009) and
26 inferred for the full 1.4 km section (Morris *et al.*, 2009; Zhao and Tominaga, 2009),
27 combined with the little deformed nature of the Site U1309 drill core suggest that at least
28 this (upper) portion of the footwall behaved as a relatively coherent block during OCC
29 formation. Flexural bending and/or sustained fault slip that enabled the rotation must

1 have resulted in fracturing, folding, or shearing in a region that is either very localized in
2 the upper 25 m of the core, which was almost unsampled, or outside the drilled zone.

3
4 Grimes *et al.* (2008) considered the issue of footwall rotation in their discussion of the
5 ages obtained from oxide gabbro and felsic dikes within the sequence (Figure 6d). They
6 suggested that the lack of systematic younging-upward ages indicates that two main
7 periods of multi-injection sill intrusions occurred at different subaxial depths (forming
8 present day rock intervals above and below ~600 mbsf, respectively). These authors then
9 investigated models of magma emplacement depth and possible active detachment fault
10 geometry to assess what the mean rock age might indicate in terms of asymmetry in
11 lithospheric extension during OCC formation. They conclude that for a minimum of a
12 few-hundred-kyr period when a detachment fault served as the main plate boundary,
13 movement of the footwall along the western ridge flank accounted for 70-100% of the
14 relative motion across the spreading axis. They inferred that the asymmetry in west
15 versus east flank spreading rates decreased over the past 1 Ma, as slip along the
16 detachment ceased.

17 18 **5c. Comparison between Hole U1309B and Upper Hole U1309D**

19 The recovered rock sequences from Holes U1309B and U1309D do not correlate simply
20 (Blackman *et al.*, 2006; Figures 4a-b). The lateral scale of thin, inter-fingered gabbroic
21 units sampled in each hole therefore must be less than the 20-m offset between holes, or
22 disruption with a significant vertical component separates the two areas. The thin
23 harzburgite unit recovered at 60 mbsf from Hole B is not directly equivalent to the
24 peridotite recovered from 62 mbsf in Hole D, which is wehrlitic (Blackman *et al.*, 2006;
25 Tamura *et al.*, 2008; Godard *et al.*, 2009). However, phenocryst alignment and downhole
26 patterns of magnetic susceptibility suggest that some of the diabase units trend upward
27 from Hole B and are intersected at depths ~11 m shallower by Hole D to the north
28 (Blackman *et al.*, 2006). This indicates that diabase units within the domal core can
29 sometimes be laterally continuous over distances greater than the size of the gabbro units

1 forming the upper 100 m at Site U1309 and that their current disposition has a component
2 of dip that is $\sim 29^\circ$ toward the south.

3 4 **5d. Conditions During Exhumation of the Domal Core**

5 The signatures of changing pressure/temperature conditions, and the extent of fracturing
6 within the domal core as unroofing and uplift proceeded are recorded as alteration
7 assemblages in the footwall rocks. All rocks in the massif have experienced the complete
8 range of metamorphic temperatures from magmatic to ambient conditions, so the
9 distribution of metamorphic assemblages documented by Blackman *et al.*, (2006) reflects
10 a combination of the timing of fluid access and the time spent in different temperature
11 intervals. Note that the discussion of facies in this paper follows common usage in
12 studies of ocean floor metamorphism (i.e., hornblende-bearing metamorphic rocks are
13 typically referred to as amphibolite, while actinolite-bearing rocks are referred to as
14 greenschist). This usage, in part, reflects the difficulty of obtaining accurate temperature
15 and pressure estimates in low-pressure rocks where water activity can vary widely in both
16 time and space.

17
18 Granulite and upper amphibolite-facies ductile deformation was extremely limited, and
19 more or less confined to the upper part of the sequence (Figures 4d and 9c). These shear
20 zones have not been thoroughly studied, but likely formed at temperatures in excess of
21 750 °C.

22
23 Static hydration began in the amphibolite facies, continued in the greenschist facies, and
24 was pervasive in the upper part of the sequence, above about 300 mbsf (present-day
25 depth), where reactions such as tremolite-chlorite corona formation between olivine and
26 plagioclase generally continued until one of the reactant phases was consumed. The
27 intensity of both mineralogical and isotopic alteration decreases significantly below this
28 depth, and completely fresh gabbros are common beneath the fault zone at 750 mbsf
29 (Figures 4 and 8). At these depths, fluid access was restricted to faults (eg. Hirose and

1 Hayman, 2008; Michibayashi *et al.*, 2008), veins, and igneous contacts (e.g., resulting in
2 serpentization of parts of olivine-rich troctolite layers). The concentration of alteration
3 in the vicinity of late felsic intrusions may also reflect exsolution of magmatic fluids.

4
5 Additional data is required to establish the full distribution of amphibolite vs greenschist
6 facies hydration within the sequence (e.g., Nozaka and Fryer, 2011), but most samples
7 studied to date contain amphibole showing a wide range of composition reflecting a
8 broad range of temperature conditions (e.g., Blackman *et al.*, 2006; Michibayashi *et al.*,
9 2008). Alteration halos (Figure 10a,b) around several veins/igneous contacts from depths
10 433-1376 mbsf have been studied in detail by Nozaka and Fryer (2011). The halos are
11 zoned with tremolite pseudomorphs after olivine present throughout the inner zone, some
12 overgrown by green hornblende, and thick chlorite along adjacent plagioclase boundaries.
13 Talc replacement of olivine is typical within the second zone. The third zone, most distant
14 from the vein/contact, has tremolite and chlorite along boundaries of adjacent olivine-
15 plagioclase grains and relict olivine is observed (Figure 10b). Nozaka and Fryer (2011)
16 propose that the tremolite-chlorite coronas formed at temperatures between 450 and 650
17 °C, somewhat higher than the range implied by Blackman *et al.* (2006). Overprinting
18 hornblende is interpreted to reflect a period of prograde metamorphism with temperatures
19 rising to around 750 °C. Cataclasis in the fault zone at 750 mbsf also appears to have
20 occurred in the amphibolite facies, with Michibayashi *et al.* (2008) estimating an
21 amphibole-plagioclase temperature of 640 °C. Microrodingite assemblages (Figure 10d)
22 that postdate corona formation occurred below 350 °C (Frost *et al.*, 2008), while initial
23 serpentization involving antigorite may have occurred above 300 °C, continuing to lower
24 temperatures with growth of lizardite and magnetite replacing early Fe-bearing brucite
25 (Figure 10e, Beard *et al.*, 2009). Tremolite-talc veins in ultramafic horizons in the upper
26 part of the core (Figure 9b) show similar assemblages to detachment fault rocks (Escartin
27 *et al.*, 2003; Boschi *et al.*, 2006). Talc at the edge of the vein in Figure 9b contains
28 magnetite inclusions, suggesting it replaced serpentine. This may also have been a
29 prograde event, although further work is required to establish this.

1
2 Hydration at temperatures below 250-300 °C was restricted to late clay filled fractures,
3 that are most abundant below about 400 mbsf (Nozaka *et al.*, 2008), and to zeolites which
4 are fairly abundant below 700 mbsf (Figure 4), but have not been proved by XRD at
5 shallower levels. Saponitic clay and zeolites probably reflect ambient conditions (Nozaka
6 *et al.*, 2008), where temperatures of at least 120 °C are present at 1400 mbsf (Blackman
7 *et al.*, 2006). The predominance of alteration at temperatures >250 °C is confirmed by the
8 lack of whole rock $\delta^{18}\text{O}$ values greater than +5.5 ‰ (McCaig *et al.*, 2010). Sr isotopic
9 alteration is most intense in gabbroic rocks, tremolite schists and serpentinites in the
10 upper 100 m of the core (McCaig *et al.*, 2010, and Figure 8c), suggesting relatively high
11 fluxes of seawater-derived fluids in this zone.

12
13 Pervasive alteration in the upper part of the sequence occurred mainly under decreasing
14 temperature conditions in the amphibolite and upper greenschist facies (Blackman *et al.*
15 2006), with alteration penetrating further from the detachment fault with time. This may
16 have been mainly lateral penetration away from a steep detachment fault at the time of
17 alteration (Figure 10f). Nozaka and Fryer (2011) suggest that green hornblende
18 overprinting tremolite within the zoned halos below 350 mbsf indicates prograde
19 metamorphism after initial hydration. Talc and perhaps tremolite apparently replacing
20 serpentine (Figure 9b) may also reflect a prograde event in the upper part of the sequence.
21 The fact that late diabase and basalt intrusions chill against amphibole-rich breccias of
22 metagabbro and metadiabase shows that magmatism and hydrothermal activity were
23 occurring at nearly the same time. Prograde events may reflect either the direct effects of
24 intrusions or flow of hot fluids related to intrusions at depth (Nozaka and Fryer, 2011).
25 McCaig *et al.*, (2010) suggest that flow of hydrothermal fluids through the fault zone
26 buffered temperatures to around 400 °C, promoting rapid initial cooling of the footwall
27 from magmatic temperatures but slower cooling through the amphibolite and upper
28 greenschist interval (Figure 10f). Rapid final exhumation of the massif onto the seafloor
29 quickly established an ambient thermal gradient of around 100 °C/km, leading to the

1 cessation of metamorphism in the upper part of the sequence and growth of clays and
2 zeolites at deeper levels.

3
4 Radial micro-fractures localized around altered olivine grains indicate that volume
5 increase associated with serpentinization enhances general seawater access into gabbroic
6 rocks (Blackman *et al.*, 2006, Nozaka *et al.*, 2008). Similar volume increase appears to
7 have promoted both the tremolite-chlorite corona textures in troctolite (Blackman *et al.*,
8 2006), and perhaps the serpentine-microroddingite “ladder veins” described by Frost *et al.*,
9 2008). Reaction-enhanced permeability caused by volume increase reactions may have
10 promoted pervasive access of fluid to relatively unfractured rocks, but the locally
11 enhanced hydration along narrow shear zones indicates that significant fluid flow is
12 confined to these intervals (Hirose and Hayman, 2008). The juxtaposition of highly
13 altered zones against intervals showing little or no alteration is important. Specific
14 examples include (Figure 4): the moderately fresh olivine gabbro interval at 380-400
15 mbsf, the sharp contrast in alteration of the 1090-1235 mbsf olivine-rich interval and
16 gabbro on either side, and the presence of some very fresh gabbro and olivine-rich
17 troctolite samples within this olivine-rich troctolite zone. Sharp contrasts in borehole
18 resistivity also suggest such juxtaposition of highly altered rock and intervals with little
19 metamorphism (Figure 4e, depths of 380, 750, and 1080 mbsf, where jumps of an order
20 of magnitude (ohm-m) occur across 5-15 m length intervals). Hirose and Hayman (2008)
21 propose that this pattern of alteration requires that fluid flow is either restricted to zones
22 that are very narrow (cms to ~1 m), and/or that a self-sealing mechanism accompanies
23 fluid transfer in the fractured zones.

24 25 **6. Implications of Drilling Results**

26 Following a synopsis of the inferences about the structure, lithology, and evolution of
27 Atlantis Massif drawn from our post-drilling analyses, we discuss the extent to which
28 drilling results addressed the initially-targeted hypothesis tests, as well as some additional
29 implications for the site and comparison with other deep drilling results at OCC.

- The main geochemical characteristics of Site U1309 gabbroic rocks are consistent with formation as a cumulate sequence built from a series of parental MORB melt injections (Godard *et al.*, 2009). Self-intrusion of cooling, partially crystallized magma likely occurred, and infiltration of evolved melt from a given intrusion into pre-existing mafic cumulate rock certainly occurred.
- The age of zircon-bearing core samples (Grimes *et al.*, 2008) is consistent with formation in the axial zone and a period of asymmetric spreading, with the footwall to a detachment fault moving at or near the full spreading rate for segment.
- The few thin peridotite intervals transected at Site U1309 are residual, but petrographic and geochemical evidence indicate later-formed or injected melts fluxed the residuum (Godard *et al.*, 2009) or infiltrated it as dikelets (Tamura *et al.*, 2008).
- Olivine-rich troctolites are the product of intense melt-rock interactions between an olivine-rich protolith (either ultramafic cumulate or mantle peridotite) and basaltic melt (Suhr *et al.*, 2008 ; Drouin *et al.*, 2009, 2010). They cannot simply be the primitive, first-crystallized cumulate within cooling magma. Such melt-rock interaction processes are expected to play a significant role in crustal accretion at slow-spreading ridges, hence to contribute through melt-rock interactions to MORB chemistry (Lissenberg and Dick, 2008; Drouin *et al.*, 2010).
- A distinct decrease in alteration with depth indicates pervasive seawater infiltration only in the upper ~380 m. The consistent >40%, low temperature alteration in the upper section gives way to moderate levels of alteration in the interval 400~750 mbsf (Blackman *et al.*, 2006). Below 800 m, alteration is quite localized and many intervals are very fresh. This indicates that fracturing and seawater infiltration associated with core complex formation does not occur equally throughout the whole young lithosphere. Rather, the highest water-rock ratios are recorded in the now-exposed detachment zone (McCaig *et al.*, 2010) and alteration at depth is confined to local zones (Nozaka and Fryer, 2011).

- Paleomagnetic data indicate at least 45° anti-clockwise rotation of the footwall with tilt occurring about a MAR-parallel horizontal axis (Morris *et al.*, 2009).

Table 2 charts the sequence of processes and conditions that the drilled section experienced, as constrained by shipboard and post-cruise results.

Returning to the objectives laid out for the IODP Expeditions to Atlantis Massif, our results provide a test of many, but not all, of the hypotheses outlined in Table 1.

Hypotheses 1, 2, and 5: Any high-strain portion of the detachment zone at Site U1309 appears to be less than 25 m thick, as we recovered few strongly deformed fault rocks from the 1415 mbsf interval cored. While only a few fragments of fault rock were actually recovered within a few meters of the seafloor, we cannot rule out the possibility that we simply did not recover a potentially greater amount of likely fragile rock, due to difficult conditions that prevail when starting a deep hole with a drilling vessel. Seismic tomography (Collins *et al.*, 2009; Blackman *et al.*, 2009; Figure 3) indicates that a low velocity top interval about 100 m thick characterizes at least parts of the Central Dome. The reduced velocity could be explained by alteration and/or brecciation within a broader detachment zone although we cannot rule out increased porosity associated with exposure at the seafloor.

Paleomagnetic data confirm that the footwall to the detachment fault likely rotated >45° (Morris *et al.*, 2009), consistent with a rolling hinge model and flexural rotation (e.g., Wernicke and Axen, 1988; Buck, 1988). Fully oriented samples are not available in the upper ~100 m and analysis is still underway for the 400-1400 m interval, although inclinations for the latter are consistent with this interpretation. If the proportion of serpentinitized peridotite recovered from Hole U1309D is representative of the bulk composition of Atlantis Massif, expansion of altered peridotite does not contribute significantly to uplift of the Central Dome

1
2 *Hypothesis 3:* The lack of extrusive rock or another cap rock above the intrusive complex
3 at Site U1309 confirms that at least some unroofing has occurred. While current results
4 do not pin down the depth of emplacement, the rocks clearly were intruded deep enough
5 for slow crystallization. The alteration history (Nozaka *et al.*, 2008; 2011; McCaig *et al.*,
6 2010) indicates rapid cooling through the granulite facies, followed by slower cooling
7 through amphibolite and greenschist facies. This was followed by rapid uplift, to
8 conditions where zeolite facies metamorphism prevailed under ambient conditions in the
9 lower part of the Hole U1309D sequence.

10
11 *Hypothesis 4:* Expeditions 304/305 mark the third time that deep drilling of a corrugated
12 oceanic core complex produced a significant thickness of gabbro in an area where mantle
13 ultramafic rocks are exposed on the seafloor nearby (Dick *et al.*, 2000, Kelemen *et al.*,
14 2007). This led to our revised model of OCC formation (Ildefonse *et al.*, 2007a), which
15 predicts that a local increase in magma supply to a portion of the segment that is normally
16 less magmatically robust is an important factor in long-lived strain localization within the
17 axial zone. A series of melt injections at depth, over a period of at least a few hundred kyr
18 (Grimes *et al.*, 2008), is hypothesized to form a gabbroic body that behaves rather
19 coherently. Strain is focused around the margins of the composite ‘batholith’ where
20 alteration by fluids locally reacting with surrounding peridotite country rock significantly
21 reduces its strength (Escartin *et al.*, 2001; Jöns *et al.*, 2009; Nozaka and Fryer, 2011).

22
23 While the drilling results were a basis for the Ildefonse *et al.* (2007a) hypothesis, a
24 number of questions remain. The multi-km scale of the domal cores of many OCC
25 suggests that the size of the gabbroic body is comparable, if the ‘ball bearing’ analogy is
26 appropriate. Seismic tomography of the upper ~1.5 km (Canales *et al.*, 2008; Henig *et al.*,
27 2009) confirms that shallow high-velocity, such as would typify mafic intrusive rock, is
28 present within the domal core of Atlantis Massif. However, this velocity-depth signature
29 does not extend the full cross-strike length of the OCC’s core. Recent numerical

1 modeling (Buck et al., 2005; Tucholke et al., 2008) may provide a framework for
2 interpreting this variability if the velocity structure documents a level of magmatism
3 accommodating 30-50% of spreading while large-offset faulting takes up the rest. Note
4 that samples from the conjugate crust on the outside corner across from Atlantis Massif
5 have not yet been obtained. These will be crucial for understanding how magma may or
6 may not have been partitioned within the axis or with respect to the detachment fault.

7
8 *Hypothesis 6:* Reanalysis of geophysical data (Blackman *et al.*, 2008; Canales *et al.*,
9 2008; Collins *et al.*, 2009; Henig *et al.*, 2009) indicates that there is not a shallow (< 1
10 km) regional Moho at Atlantis Massif. Since the seismic boundary was not transected, we
11 cannot address its geologic properties. As noted in Section 4, the lateral heterogeneity
12 that characterizes slow-spread crust, particularly at OCC, invalidates some of the
13 simplifying assumptions that often influence initial marine geophysical modeling. More
14 in-depth analysis of the pre-drilling geophysical data would have clarified the range of
15 viable interpretations. This could have aided decision making, and, assuming the
16 experiment was still high priority, may have suggested alternate/additional strategies for
17 drilling/logging.

18
19 *Hypothesis 7:* The recovery of 1415 m of gabbro from the Central Dome, where seismic
20 velocities in the upper ~ 1 km are found to be higher than normal for young Atlantic crust
21 (Canales *et al.*, 2008), and the similarity of the velocity structure determined for the
22 eastern part of the Southern Ridge (Henig *et al.*, 2009), where the largest residual gravity
23 anomaly is found (Blackman *et al.*, 2008), indicates that fresh peridotite is not the source
24 of the gravity high. Instead it is the fact that intrusive mafic rock, whose inherent porosity
25 is lower than typical upper crustal volcanic rock, is exposed at the seafloor within the
26 Central Dome. Both the porosity contrast and the greater density of gabbro compared to
27 basalt contribute to the relative anomaly between the dome and the adjacent hanging wall
28 blocks.

1 The inclusion of very thin screens of mantle peridotite within the km-scale gabbroic
2 sequence drilled at IODP Site U1309, in combination with the bulk composition of the
3 Hole not being the more primitive cumulate complement of MORB sampled in the
4 current median valley documents the complexity of slow-spread lithosphere formation/
5 evolution. Models where the large majority of basaltic melt formed during subaxial
6 partial melting migrates to eventually reside in a separate overlying, upper crustal layer
7 must be modified. Some melt appears to be left behind and reacts with its matrix
8 minerals. While we cannot rule out incorporation of some of the thin mantle screens as
9 fault slivers, the impregnation and reactions observed within the olivine-rich troctolite
10 intervals indicate that deep lithosphere forming within the axial zone can be infused with
11 injections of melt. Drilling results at Atlantis Massif support models where emplacement
12 of gabbroic plutons within slow-spread ocean lithosphere (e.g., Cannat, 1993) is
13 accompanied/ followed by faulting (Cannat *et al.*, 1997, Lagabrielle *et al.*, 1998), which
14 eventually exposes these rocks at the seafloor. The degree (cumulatively, ~3:1
15 melt:residual ratio) and scale (intervals occur within zones that extend a few tens of
16 meters) of impregnation observed within the upper 1.4 km at Site U1309 suggest an axial
17 region where intrusions exceeded deformation of mantle lithosphere under amagmatic
18 conditions. This type of constraint has not previously been clear for an OCC, where the
19 genesis of material contained in footwall is key to understanding the interplay between
20 magmatism and tectonism during its evolution.

21
22 Despite undergoing major faulting, rotation, and significant uplift, the domal core of
23 Atlantis Massif is not pervasively deformed or altered. The interplay between fluid
24 circulation (alteration) and strain localization acted to protect large portions of the
25 shallow lithosphere. Metasomatism appears to concentrate along the detachment fault
26 zone and the boundaries between gabbroic and peridotite host rocks (Bach and Klein,
27 2009; Boschi *et al.*, 2006, McCaig *et al.*, 2007) rather than permeating throughout the
28 footwall to the detachment.

1 The first-order similarity of OCC's that have been drilled to date by ODP and IODP is the
2 occurrence of gabbro plutons in the domal core (Ildefonse *et al.* (2007a,b). The most
3 spectacular difference between the Atlantis Bank OCC in the Indian Ocean (Dick *et al.*,
4 2000), and the OCCs in the Atlantic (15°45'N, and Atlantis Massif) documented by
5 shallow coring (MacLeod *et al.*, 2002) and/or deep drilling (Blackman *et al.*, 2006;
6 Kelemen *et al.*, 2007) is the proportion of crystal-plastic deformation recorded in the
7 gabbroic sequence; the core from ODP Hole 735B (Atlantis Bank; Dick *et al.*, 2000)
8 displays a thicker (up to many tens of meters) protomylonitic to mylonitic shear zone at
9 the top of the section, as well as many more shear zones down section. In contrast,
10 deformation in cores from Atlantic OCCs, in particular in samples from directly beneath
11 detachment faults, occurred at much colder conditions (Escartin *et al.*, 2003; Ildefonse *et*
12 *al.*, 2007a; Miranda and Dilek, 2010; McCaig *et al.*, 2010). The contrasted metamorphic
13 and deformation history can be summarized in a simple typology of OCCs (Escartin *et*
14 *al.*, 2003; Miranda and Dilek, 2010; McCaig *et al.*, 2010), with the Atlantis Bank
15 representing a “hot” end-member for detachment faults with extensive mylonitization at
16 temperatures >800 °C (Dick *et al.*, 2000; Mehl and Hirth, 2008; Miranda and John,
17 2010), while the Atlantis Massif and 15°45'N represent a “cold” end-member where
18 gabbro was intruded into the roots of a hydrothermal system controlled by the
19 detachment fault. The greater extent of mylonitic deformation in gabbroic rocks on the
20 South Wall of the Atlantis massif (Schroeder and John, 2004; Karson *et al.*, 2006; see
21 also section 7.1) would then be explained by the intrusion of the Central Dome gabbro
22 after and across this ductile shear zone that represents deeper parts of the detachment
23 fault (McCaig *et al.*, 2010). An alternate to this characterization put forward by John and
24 Cheadle (2010) suggests that the presence or absence of zones of high strain mylonite is
25 likely dictated by several factors including position relative to the breakaway (i.e., initial
26 structural depth), magnitude of slip, rheology (whether dominated by mafic or felsic
27 rocks types), and the involvement of water promoting plastic deformation, during fault
28 zone evolution.
29

7. Drilling Results in the Context of Regional Data

7.1. Comparisons between Southern Ridge and Central Dome

There are significant differences in seafloor depth, lithology, deformation, and alteration between the Central Dome and the well-mapped face of the central part of the Southern Ridge of Atlantis Massif (Figures 1, 2; Schroeder and John, 2004, Boschi *et al.*, 2006, Karson *et al.*, 2006). Whereas serpentinitized harzburgite constitutes <1% of the sequence recovered at Site U1309, serpentinitized harzburgite composes >50% of the sample suite obtained by submersible/dredging on the south wall (Blackman *et al.*, 2002; Boschi *et al.*, 2006). Delacour *et al.* (2008) and McCaig *et al.* (2010) evaluated Sr and Nd ratios for Site U1309 and several south wall samples. They note that high fluid flow with associated alteration and strain localization characterize the South Wall samples but is less intense within the Central Dome sequence sampled. Based on widespread talc-amphibole-chlorite assemblages within the detachment shear zone atop the Southern Ridge, Boschi *et al.* (2006) conclude that extensive metasomatism accompanied deformation that varied from crystal-plastic to cataclastic in this zone. Boschi *et al.* (2006) emphasize the importance of mafic-ultramafic interactions in such high exchange zones where deformation occurred in the ~100 m thick detachment shear zone capping the South Wall (Schroeder and John, 2004, Karson *et al.*, 2006). If an exposed detachment caps the Central Dome, shearing associated with its displacement would have to have been significantly more localized. A lack of significant ultramafic rock in the Central Dome region would be expected to play an important role in such difference. Some strain may also have partitioned into breccia zones within the gabbro, the thickness of which may be underestimated due to poor recovery and overprinting by undeformed diabase/basalt intrusions. Constraints on the thickness of detachment-related deformation across the southeast shoulder are currently lacking.

Published tomographic models of refractions recorded on the MCS streamer also document along-strike variability within the domal core. Canales *et al.* (2008) show that

1 shallow compressional wave velocities are generally high (5.5-6.5 km/s) in the middle
2 and eastern flank of the Central Dome, and gradients in the upper few hundred meters
3 exceed that of average young Atlantic crust (White *et al.*, 1992; compare curves to gray
4 shaded region in Figure 3e). In comparison, the central section of the Southern Ridge,
5 where MCS Line 4 crosses (location in Figure 2), has gradients in the upper km that are
6 typical of young Atlantic crust and velocity is lower (3.5-4.5 km/s; Figure 3d-e). This part
7 of the Southern Ridge has shallow velocity structure similar to the western flank of the
8 Central Dome. Geologic mapping, geochemistry and these seismic results led to a
9 previously-proposed model that predicts the Southern Ridge consists dominantly of
10 altered ultramafic rocks in contrast to the mafic-dominated Central Dome (Karson *et al.*,
11 2006; Canales *et al.*, 2008). The few-km scale of shallow velocity variability observed
12 within Atlantis Massif is similar to what has been documented in the upper ~1 km at the
13 Kane OCC (Xu *et al.*, 2009).

14
15 While along-strike heterogeneity clearly exists within the footwall of the Atlantis Massif
16 OCC, additional seismic analysis shows that significant cross-strike heterogeneity also
17 occurs within the Southern Ridge. New tomographic results for MCS Line 9 (Henig *et al.*,
18 2009), which crosses the entire Southern Ridge (Figure 2), and had not previously
19 been studied in detail, indicate that the southeast shoulder may be more similar to the
20 Central Dome. High seismic velocity and steep gradients at shallow depths characterize
21 this area; velocity-depth profiles for the southeast shoulder portion of Henig's
22 tomography model plot with the solid curves for Lines 10 and 4 in Figure 3e.

23
24 The Southern Ridge has a doubly plunging corrugated surface, although the south-
25 dipping portion only exists on the southeast shoulder today (Figure 2). Presumably the
26 extension of this surface to the south of the present-day peak of the massif, at the center
27 of the Southern Ridge, has undergone mass-wasting with the arcuate headwall scarps at
28 the top of the South Wall demonstrating this process (Blackman *et al.*, 2002; Karson *et al.*,
29 2006). Applying the structural projection of Schroeder and John (2004), all mapping

1 and sampling to date on the Southern Ridge is located less than ~500 m below the paleo-
2 detachment. Thus, current understanding of the 3-D geometry of the detachment fault
3 system is limited to the upper half kilometer in what is a multi-km (vertical and lateral)
4 tectonic feature. The upper section is unquestionably crucial for understanding the
5 evolution of Atlantis Massif but our knowledge of the deeper levels of the core complex
6 remains limited. While the seafloor dominance of serpentinitized harzburgite at the top of
7 the South Wall is certain, the subseafloor extent of this rock type is not yet proven.
8 Canales' *et al.* (2008) seismic interpretation that the central Southern Ridge is dominantly
9 serpentinitized peridotite is quite reasonable given the rock types exposed on the upper
10 South Wall. However, it is also true that the velocity structure is typical of average young
11 Atlantic crust (Figure 3e), which could point toward fractured mafic crust underlain by
12 competent, mainly gabbroic lower crust. The model of Ildefonse *et al.* (2007a) raises the
13 possibility that what has been sampled to date on the South Wall represents a sheath of
14 deformed rock, dominantly altered peridotite, which surrounds gabbroic plutons at the
15 core of the OCC. The recently-recognized higher seismic velocities in the southeast
16 shoulder (Henig *et al.*, 2009) may support such an inference. Geologic data on the eastern
17 part of the Southern Ridge are sparse. Of 14 Alvin samples from dive 3647 there, two are
18 talus samples of serpentinitized peridotite and six each are gabbro and metabasalt
19 (Blackman *et al.*, 2002). A very large dredge haul containing only gabbro was recovered
20 from further down the slope (Figure 2; Cann *et al.*, 1997; Blackman *et al.*, 1998). Towed
21 video mapping on the northern flank of the southeast shoulder (location in Figure 2)
22 imaged pillow basalt. Such observations can be viewed in support of the southeast
23 shoulder being underlain dominantly by mafic rocks.

24
25 Evidence for alternatives to the Ildefonse *et al.* (2007a) hypothesis also exists at Atlantis
26 Massif. Beneath the deformed rock in the top 100 m of the Southern Ridge (Schroeder
27 and John, 2004; Karson *et al.*, 2006), the bedrock includes a fair amount of little-
28 deformed serpentinitized peridotite. It is not just gabbro that avoided strong deformation as
29 the domal core was unroofed. The seismic data alone cannot rule out the possibility that

1 the increase in cross-strike velocity and gradient from central to eastern Southern Ridge
2 is, in part, due to presence of less altered peridotite in the southeast. A small (+5-8 mGal)
3 residual gravity anomaly remains after removal of a 3-D gabbroic core contribution from
4 the Bouguer anomaly (Blackman *et al.*, 2008). Occurrence of slightly-altered peridotite
5 could produce this signal, although presence of significant oxide gabbro at shallow
6 depths could as well. Geochemical analysis of samples from the SE shoulder area was not
7 conducted for the Delacour *et al.* (2008) or Boschi *et al.* (2006) studies; such work would
8 shed light on how evolution of the Southern Ridge compares with that of the Central
9 Dome.

10 11 **7.2. Working Model for the Evolution of Atlantis Massif OCC**

12 The present drilling and regional results provide sufficient information to explore a model
13 for the evolution of Atlantis Massif OCC (Figure 11). In addition to the basic geologic
14 and geophysical constraints, we consider limits on the likely pressure/temperature of
15 magma crystallization and temperatures/fluid:rock ratios of alteration experienced by the
16 sequence as it cooled (Sections 5a, 5d, Table 2). The tectonic elements in our model are
17 guided by the observed deformation within the cored sequence (Section 5b), observations
18 along the South Wall (Section 7.1) and present-day seafloor morphology.

19
20 To develop a tectonic framework for the evolution of Atlantis Massif we need some
21 constraint on the slip history along the detachment. Pb/U zircon ages available from
22 widely-spaced samples along the South Wall, taken with the average age obtained for
23 Hole U1309D, have been used to estimate a time-integrated slip rate for the detachment
24 system of 28.7 ± 6.7 mm/yr for at least 200 kyr (Grimes *et al.*, 2008). This rate is
25 essentially the full spreading rate in this part of the MAR (Pariso *et al.*, 1996). One
26 possible model would have the detachment, inferred (on the basis that spreading parallel
27 corrugations mark relative slip between the footwall and hanging wall) to be exposed
28 across the Central Dome, slipping at rates/times that coincide with activity on the
29 detachment exposed on the Southern Ridge. Existing U/Pb zircon data are consistent with

1 this interpretation, but do not require it. For this scenario to fit Atlantis Massif, the
2 evolution of the two regions following the period when a detachment served as the main
3 locus of plate separation must differ. Uplift of the Southern Ridge uplift was greater, and
4 the western edge of the corrugated surface on the Central Dome is a few km farther west
5 than where any striations or corrugations are evident on the Southern Ridge. (Figure 1c,
6 2).

7
8 Prior to about 1.5 Ma, the ridge segment north of Atlantis Transform Fault (ATF) was
9 likely typical for a slow-spreading ridge—consistent magma supply to the center of the
10 segment and variable, often reduced supply within 15-20 km of the transform (Figure
11 11a).

12
13 An episode of enhanced melt supply (Ildefonse *et al.*, 2007a) occurred ~1.1-1.3 Ma and
14 magma was injected in the southern part of the segment (Figure 11b). These would
15 become the rocks dated by Grimes *et al.* (2008), with ages possibly biased toward the end
16 of the episode since late-stage oxide gabbro and felsic veins are the predominate rocks
17 types hosting zircon.

18
19 Steep faults at the seafloor propagated downward and connected with the weakened,
20 altered (by magmatic fluids, minor seawater; Ildefonse *et al.*, 2007a; Jöns *et al.*, 2009;
21 Nozaka and Fryer, 2011) zone surrounding the new pluton. This through-going fault zone
22 served as a conduit for seawater penetration to a significant depth (Figure 11c).

23 Localization of strain occurred as alteration further weakened this zone and the
24 detachment fault was established. High fluid flow rapidly cooled the detachment zone
25 and relative plate motion focused mainly along it for at least 0.2 m.y., perhaps more.
26 Fault slip resulted in westward offset and uplift of the footwall, with some initial rollover
27 occurring due to non-zero flexural strength of the lithosphere. This bending opened
28 (micro) fractures that allowed onset of static alteration in the upper few hundred meters
29 as the footwall was exposed.

1
2 Magmatism in the center of the segment presumably continued through the 1.5-1.1 Ma
3 period and eventually an axial volcanic ridge propagated south into the early-dome
4 portion of the segment, cutting off activity on the northern part of the detachment (~0.9
5 Ma, Figure 11d). This is the scenario proposed by MacLeod *et al.* (2009) to typify the
6 latter part of the 'life cycle' of an OCC. The paleo-axial volcanic ridge responsible for
7 causing cessation of displacement along the northern part of the detachment at Atlantis
8 Massif would be the one currently atop the eastern edge of the hanging wall block
9 (Figures 1a, c). Hummocky backscatter pattern, many closed-contour bathymetric
10 features capping the ridge, and its greater local relief compared to the low hummocks that
11 cover most the hanging wall, all support the interpretation of the ridge as a volcanic
12 chain, rather than just an upturned lip of the hanging wall block. This volcanic ridge is
13 present along much of the hanging wall edge (Blackman *et al.*, 1998) but it does not
14 extend completely along the Central Dome and certainly not to the Southern Ridge. Thus,
15 we propose that the southern part of the detachment continued to slip for somewhat
16 longer, contributing to the greater uplift of the Southern Ridge.

17
18 While the southern footwall displacement ensued as a mix of detachment-controlled
19 vertical and lateral motion, the central blocks experienced mostly horizontal motion and
20 domino-block rotation associated with en-echelon steep faults, such as Schroeder *et al.*
21 (2007) suggest to be the mode by which axial material transitions from vertical to lateral
22 motion at a slow-spread ridge with modest magma supply. Around 0.5 Ma, the southern
23 detachment was cut by a younger, steeper fault and both central and southern domal
24 highs became part of the relatively coherent lithosphere, rafting along with the overall
25 motion of the western flank of the MAR (Figure 11e).

26
27 There are aspects of Atlantis Massif that this model does not address. One is the western
28 shoulder of the Southern Ridge. Sonar and a single video run there do not appear to
29 provide conclusive indication of the rock type. Gravity analysis indicates that the overall

1 density of this part of the Southern Ridge is somewhat lower than that of the middle and
2 eastern parts (Blackman *et al.*, 2008) which, when taken with the bathymetry, might
3 suggest this area is underlain by fractured basalt. The deeper video run on the western
4 shoulder (Figure 2) imaged probable pillow basalts in a small graben where structure was
5 more visible than immediate surroundings. However, the sidescan signature of the top of
6 the western shoulder, which was characterized as ‘basement’ by Blackman *et al.* (1998),
7 is not typical of volcanic constructional seafloor. Our model for the history of slip on the
8 detachment would not, in 2-D, explain why the western shoulder is as shallow as the rest
9 of the Southern Ridge. If the transform is a relatively low-friction fault (Fox and Gallo,
10 1984), perhaps this allowed uplift of the older crust, outboard of the detachment, to occur
11 whereas it was inhibited in the Central Dome region.

12
13 Other models could also explain aspects of our current knowledge of Atlantis Massif. The
14 interpretation of Henig’s seismic results as a few-km gabbroic body in the southeast
15 shoulder could be explained by enhanced magmatic intrusion in that southernmost
16 portion of the segment, which was not coeval with the intrusions that were drilled in the
17 Central Dome. In this case, along-strike variation in the timing and duration of
18 detachment faulting would be expected and would control how morphology of the
19 Central Dome versus Southern Ridge developed. Lithology of the footwall would not
20 necessarily be similar for the Central Dome and Southern Ridge. This type of model is
21 favored for the Kane OCC (Dick *et al.*, 2008; Xu *et al.*, 2010). In this scenario, the need
22 for the transform to play a role in allowing enhanced uplift of the Southern Ridge is
23 removed, since this dome evolves independent of the Central Dome. The steep scarp on
24 the eastern side of the Southern Ridge could then represent a fault termination of this
25 detachment. Cannat *et al.* (2009) note that steep scarps bound the young side of many
26 OCC on the flanks of the southwest Indian ridge. They propose that these mark steep
27 faults that terminate slip on the detachment system, as plate rigidity transitions from a
28 period of localized weakness to generally greater strength.

1 To test between the model we propose and others, comparison of the petrologic and
2 geochemical signatures of the Central Dome and southeast shoulder gabbros is a
3 worthwhile starting point that could begin immediately with existing samples. Additional
4 subseafloor sampling would improve the strength of such investigation. Detailed
5 comparison of the seismic properties within the Central Dome and Southern Ridge can
6 also shed more light. The downward-continued MCS refraction data provide the most
7 robust results throughout the interval covered, and comparison of different portions of the
8 footwall is a component of work that is currently underway for Atlantis Massif (Henig *et*
9 *al.*, 2009). Future data that could test between models include oriented paleomagnetic
10 samples across the Southern Ridge, to compare any rotation with that documented in the
11 Central Dome. Our model predicts somewhat greater rotation of the former than the
12 latter; the Cannat *et al.* (2009) model might predict less rotation for the Southern Ridge.
13 Seismic velocity measurements of the lithosphere across the Southern Ridge and
14 conjugate crust at 1.5-8 km depths would allow comparison of vertical and lateral
15 structure to that obtained along an existing 40-km refraction profile across the Central
16 Dome (Blackman and Collins, 2010).

17 18 **8. Conclusions**

19 The results obtained through analysis of the IODP data from Atlantis Massif provided
20 fundamental new insights on the formation and evolution of the oceanic core complex at
21 this site. Some of the findings required that prior interpretations of the structure of
22 Atlantis Massif be revised. In particular, the Central Dome was shown to be dominantly
23 mafic, rather than ultramafic; more in-depth geophysical analyses were inspired and
24 produced models that are consistent with this petrologic result. The geologic inferences
25 available at the drill site can be extended using the regional survey data that also cover
26 the Southern Ridge of the massif, where seafloor mapping is fairly extensive. With this
27 along-strike view, it is clear that differences in the extents of magmatic intrusion along
28 the axis and/or the timing and duration of detachment fault activity must have shaped the
29 evolution of the massif. The working model that we put forth includes mechanisms for

1 producing along/across strike variability that differ somewhat from prior models
2 developed for the Kane (Dick et al., 2008; Xu et al., 2010) and 13°N MAR (MacLeod et
3 al., 2009) core complex regions; each of these models warrant further testing as
4 additional data become available.

5
6 The relatively continuous sampling with depth provided by the drill core was crucial for
7 understanding the nature of magmatic intrusions that built the domal core at Atlantis
8 Massif. High recovery enabled assessment of the extents and styles of alteration
9 associated with fluid circulation as strain localized, the detachment fault formed, and the
10 footwall was unroofed and exposed at the seafloor. The main findings from post-cruise
11 analysis of the IODP data are:

12 A series of magmatic intrusions formed the rocks recovered by drilling in the upper
13 1.4 km of the footwall to the exposed detachment fault. Pre-existing ultramafic rocks
14 were fluxed by melt; the recovered olivine-rich troctolites appear to be residual
15 mantle peridotite lenses that experienced such flux but whose volume in this part of
16 the footwall is rather limited (a few percent of the total sequence).

17 Little deformation is recorded in the drill core and what occurs is quite localized.
18 While brecciation and alteration patterns in the top 80 m may indicate a broader zone
19 of shearing, rare schist fragments, inferred to mark the exposed detachment fault,
20 were recovered but most were in the top few meters. Paleomagnetic data indicate that
21 the footwall has tilted at least 45°, supporting a rolling hinge model for core complex
22 development. Combined with the sparse and very localized deformation, this implies
23 mainly coherent behavior of the footwall to a depth of 1.5 km minimum.

24 Seawater infiltration was pervasive in the upper ~380 m, with high fluid-rock ratios
25 documented for the upper ~100 m. Alteration at greater depths is moderate and only
26 occurs in local zones below 800 mbsf, mainly near veins and igneous contacts.

27
28
29 **Acknowledgements.**

1
2 This research used samples and data provided by the Integrated Ocean Drilling Program
3 (IODP). The tomographic model in Figure 3d was kindly provided by Pablo Canales. We
4 thank Jeff Karson for his thorough and insightful review, it helped us significantly
5 improve the manuscript. An anonymous reviewer's comments on the alteration aspects
6 helped us clarify and increase the synthesis of those results.
7

8 **References.**

- 9
10 Bach, W., and F. Klein (2009), The petrology of seafloor rodingites: Insights from
11 geochemical reaction path modeling, *Lithos*, 112, 103-117. doi:10.1016/j.lithos.
12 2008.10.022.
13 Beard, J. S., et al. (2009), Onset and progression of serpentinization and magnetite
14 formation in olivine-rich troctolite from IODP Hole U1309D, *J. Petrology*, 50,
15 387-403, doi:10.1093/petrology/egp004.
16 Blackman, D. K., et al. (1998), Origin of extensional core complexes: evidence from the
17 Mid-Atlantic Ridge at Atlantis fracture zone, *J. Geophys. Res.*, 103, 21,315-21334. doi:
18 10.1029/98JB01756.
19 Blackman, D. K., et al. (2002), Geology of the Atlantis Massif (MAR 30°N): implications
20 for the evolution of an ultramafic oceanic core complex, *Mar. Geophys. Res.*, 23,
21 443-469. doi:10.1023/B:MARI.0000018232.14085.75.
22 Blackman, D. K., et al. (2004), Oceanic core complex formation, Atlantis Massif—
23 oceanic core complex formation, Atlantis Massif, Mid-Atlantic Ridge: drilling into the
24 footwall and hanging wall of a tectonic exposure of deep, young oceanic lithosphere to
25 study deformation, alteration, and melt generation, *IODP Sci. Prosp.*, 304/305, doi:
26 10.2204/iodp.sp.304305.2004.
27 Blackman, D.K., Ildefonse, B., John, B.E., Ohara, Y., Miller, D.J., MacLeod, C.J., and the
28 Expedition 304/305 Scientists (2006) Proc. IODP, 304/305: College Station TX
29

- (Integrated Ocean Drilling Program Management International, Inc.) doi:10.2204/iodp.proc.304305.2006.
- Blackman, D. K., et al. (2008), Three-Dimensional Structure of Oceanic Core Complexes: Effects on Gravity Signature and Ridge Flank Morphology, Mid-Atlantic Ridge 30°N, *Geochem. Geophys. Geosyst.*, 9(Q06007), doi:10.1029/2008GC001951.
- Blackman, D. K., et al. (2009), Geophysical signatures of oceanic core complexes, *Geophys. J. Intl.*, 178, 593–613, doi: 10.1111/j.1365-246X.2009.04184.x.
- Blackman, D.K. and J.A. Collins (2010), Lower Crustal Variability and the Crust/Mantle Transition at the Atlantis Massif Oceanic Core Complex, *Geophys. Res. Lett.*, 37, L24303, doi:10.1029/2010GL045165.
- Bonatti, E., and J. Honnorez (1976), Sections of the Earth's crust in the equatorial Atlantic, *J. Geophys. Res.*, 81, 4104-4116. doi:10.1029/JB081i023p04104.
- Boschi, C., et al. (2006), Mass transfer and fluid flow during detachment faulting and development of an oceanic core complex, Atlantis Massif (MAR 30°N), *Geochem. Geophys. Geosyst.*, 7, Q01004, doi:10.1029/2005GC001074.
- Buck, W. R. (1988), Flexural rotation of normal faults, *Tectonics*, 7 959-973. doi: 10.1029/TC007i005p00959.
- Buck, W. R., et al. (2005), Modes of faulting at mid-ocean ridges, *Nature*, 434, 719-723, doi:10.1038/nature03358.
- Canales, J. P., et al. (2004), Seismic reflection imaging of an oceanic detachment fault: Atlantis megamullion (Mid-Atlantic Ridge, 30°10' N), *Earth Planet. Sci. Lett.*, 222, 543-560. doi:10.1016/j.epsl.2004.02.023.
- Canales, J. P., et al. (2008), Seismic evidence for large-scale compositional heterogeneity of oceanic core complexes, *Geochem. Geophys. Geosyst.*, 9, Q08002, doi: 10.1029/2008GC002009.
- Cann, J. R., et al. (1997), Corrugated slip surfaces formed at ridge-transform intersections on the Mid-Atlantic Ridge, *Nature*, 385, 329-332. doi:10.1038/385329a0

- 1 Cannat, M., et al. (1997), Ultramafic and gabbroic exposures at the Mid-Atlantic Ridge:
2 Geological mapping in the 15° N region, *Tectonophysics*, 279, 193–214. doi:10.1016/
3 S0040-1951(97)00113-3.
- 4 Cannat, M. H. (1993), Emplacement of mantle rock in the seafloor at mid-ocean ridges, *J.*
5 *Geophys. Res.*, 98, 4163–4172, doi:10.1016/j.epsl.2009.09.020.
- 6 Cannat, M., et al. (2009), Oceanic corrugated surfaces and the strength of the axial
7 lithosphere at slow spreading ridges, *Earth Planet. Sci. Lett.*, 288, 174–183. doi:
8 10.1016/j.epsl.2009.09.020.
- 9 Collins, J., et al. (2003), Seismic velocity structure of mid-Atlantic ridge core complexes,
10 *Geophysical Research Abstracts*, EAE03-A-10390.
- 11 Collins, J. A., et al. (2009), Seismic and Drilling Constraints on Velocity Structure and
12 Reflectivity near IODP Hole U1309D on the Central Dome of Atlantis Massif, Mid-
13 Atlantic Ridge 30°N, *Geochem. Geophys. Geosyst.*, 10, Q01010, doi:
14 10.1029/2008GC002121.
- 15 Delacour, A., et al. (2008), Sr- and Nd-isotope geochemistry of the Atlantis Massif (30°N,
16 MAR): Implications for fluid fluxes and lithospheric heterogeneity, *Chem. Geol.*, 254,
17 19–35. doi:10.1016/j.chemgeo.2008.05.018.
- 18 Dick, H. J. B. (1989), Abyssal peridotites, very slow spreading ridges and ocean ridge
19 magmatism, in *Magmatism in the ocean basins*, edited by A.D.Saunders and M. J.
20 Norry, pp. 71–105, Geological Society of London, London. doi:10.1144/GSL.SP.
21 1989.042.01.06.
- 22 Dick, H. J. B., et al. (2000), A long in situ section of lower ocean crust: results of ODP
23 Leg 176 drilling at the southwest Indian Ridge, *Earth Planet. Sci. Lett.*, 179, 31–51. doi:
24 10.1016/S0012-821X(00)00102-3.
- 25 Dick, H. J. B., et al. (2008), Plutonic foundation of a slow-spreading ridge segment: the
26 oceanic core complex at Kane Megamullion, 23°30'N, 45°20'W, *Geochemistry,*
27 *Geophysics, Geosystems*, 9(Q05014), doi:10.1029/2007GC001645.

- 1 Drouin, M., et al. (2007), Origin of Olivine-Rich Troctolites From IODP Hole U1309D in
2 the Atlantis Massif (Mid-Atlantic Ridge): Petrostructural and Geochemical Study, *Eos*
3 *Trans. AGU, 88 Fall Meet. Suppl.*(52), Abstract T53B-1300.
- 4 Drouin, M., et al. (2009), In situ geochemistry of olivine-rich troctolites (IODP Hole
5 U1309D, Atlantis Massif, Mid-Atlantic Ridge, 30°N): a record of magmatic
6 impregnation in the lower oceanic crust, *Chem. Geol.*, 264, 71-88, doi:10.1016/
7 j.chemgeo.2009.02.013.
- 8 Drouin, M., et al. (2010), A microstructural imprint of melt impregnation in slow
9 spreading lithosphere: Olivine-rich troctolites from the Atlantis Massif, Mid-Atlantic
10 Ridge, 30°N, IODP Hole U1309D, *Geochem. Geophys. Geosyst.*, 11(Q06003), doi:
11 10.1029/2009GC002995.
- 12 Escartín, J., et al. (2001), Strength of slightly serpentized peridotites: implications for
13 the tectonics of oceanic lithosphere, *Geology*, 29, 1023-1026. doi:10.1130/0091-7613
14 (2001)029<1023:SOSSPI>2.0.CO;2.
- 15 Escartín, J., et al. (2003), Constraints on deformation conditions and the origin of oceanic
16 detachments, the Mid-Atlantic Ridge core complex at 15°45'N, *Geochem., Geophys.,*
17 *Geosyst.*, 4(8), 1067, doi:10.1029/2002GC000472.
- 18 Fox, P.J. and D.G. Gallo, A tectonic model for ridge-transform ridge plate boundaries:
19 implications for the structure of oceanic lithosphere, *Tectonophysics*, 104, 205, 1984.
- 20 Frost, B. R., et al. (2008), The formation of microrodingites from IODP Hole U1309D:
21 Key to understanding the process of serpentinization, *J. Petrol.*, 49, 1579-1588, doi:
22 10.1093/petrology/egn038.
- 23 Fröh-Green, G. L., et al. (2003). 30,000 years of hydrothermal activity at the Lost City
24 vent field, *Science*, 301: 495-498.
- 25 Garcés, M., and J. S. Gee (2007), Paleomagnetic evidence of large footwall rotations
26 associated with low-angle faults at the Mid-Atlantic Ridge, *Geology*, 35(3), 279-282,
27 doi:10.1130/G23165A.
- 28
29

- 1 Godard, M., et al. (2009), Geochemistry of long in-situ section of intrusive slow-spread
2 oceanic lithosphere: results from IODP Site 1309 *Earth Planet. Sci. Lett*, 279, 110-122,
3 doi:10.1016/j.epsl.2008.12.034.
- 4 Grimes, C. B., et al. (2008), Protracted construction of gabbroic crust at a slow spreading
5 ridge: constraints from $^{206}\text{Pb}/^{238}\text{U}$ zircon ages from Atlantis Massif and IODP Hole
6 U1309D (30°N, MAR), *Geochem. Geophys. Geosys.*, 9, doi:10.1029/2008GC002063.
- 7 Harding, A. J., et al. (2007), A new method for MCS refraction data analysis of the
8 uppermost section at a Mid-Atlantic Ridge core complex, *Eos Trans. AGU*, 88(52)(Fall
9 Meet. Suppl.), Abstract S12A-03.
- 10 Henig, A. S., et al. (2009), Seismic Velocity Variation within the Footwall of an Oceanic
11 Core Complex— Atlantis Massif, Mid-Atlantic Ridge 30°N, *InterRidge Newsletter*, 18,
12 9-13, <http://www.interridge.org/IRNewsletter>.
- 13 Hirose, T., and N. W. Hayman (2008), Structure, permeability, and strength of a fault
14 zone in the footwall of an oceanic core complex, the Central Dome of the Atlantis
15 Massif, Mid-Atlantic Ridge, 30°N, *J. Struct. Geol.*, 30, 1060-1071, doi:10.1016/j.jsg.
16 2008.04.009.
- 17 Ildefonse, B., et al. (2007a), Oceanic Core Complexes and Crustal Accretion at Slow-
18 Spreading Ridges *Geology*, 35(7), 623-626, doi: 10.1130/G23531A.1.
- 19 Ildefonse, B., et al. (2007b), Deep sampling of the crust formed at Mid-Ocean Ridges:
20 scientific ocean drilling provides 'in-depth' perspective, *Oceanography*, 20, 22-33.
- 21
- 22 John, B.E., 1987, Geometry and evolution of a mid-crustal extensional fault system:
23 Chemehuevi Mountains, southeastern California: Geol. Soc. London Special Paper No.
24 28, p. 313-335.
- 25
- 26 John, B. E., et al. (2009), Data report: spatial and temporal evolution of slow spread
27 oceanic crust—graphic sections of core recovered from IODP Hole U1309D, Atlantis
28 Massif, 30°N, MAR (including Pb/U zircon geochronology and magnetic remanence
29 data). In Blackman, D.K., Ildefonse, B., John, B.E., Ohara, Y., Miller, D.J., MacLeod,

1 C.J., and the Expedition 304/305 Scientists, Proc. IODP, 304/305: College Station, TX
2 (Integrated Ocean Drilling Program Management International, Inc.). doi:10.2204/
3 iodp.proc.304305.205.2009.

4 John, B. E. and M. J. Cheadle (2010), Deformation and alteration associated with oceanic
5 an continental detachment fault systems: Are they similar?, in *Diversity of*
6 *Hydrothermal Systems on Slow Spreading Ocean Ridges*, P. Rona, et al. (eds.),
7 *Geophys. Mono.* 188, 175-206, AGU, Washington D.C.

8 Jöns, N., W. Bach, T. Schroeder, Formation and alteration of plagiogranites in an
9 ultramafic-hosted detachment fault at the Mid-Atlantic Ridge (ODP Leg 209), *Contrib.*
10 *Mineral. Petrol.* 157, 625-639, doi:10.1007/s00410-008-0357-2.

11 Karson, J. A., and D. Elthon (1987), Evidence for variations in magma production along
12 oceanic spreading centers: a critical appraisal, *Geology*, 15, 127-131. doi:
13 10.1130/0091-7613(1987)15<127:EFVIMP>2.0.CO;2.

14 Karson, J. A., et al. (1997), *Proc. ODP Scientific Results*, 153, Ocean Drilling Program,
15 College Station, TX.

16 Karson, J. A. (1990), Seafloor spreading on the Mid-Atlantic Ridge: implications for the
17 structure of ophiolites and oceanic lithosphere produced in slow-spreading
18 environments, , in *Proceedings of Symposium Troodos 1987*, edited by J. Malpas, pp.
19 547-553, Geological Survey Dept., Nicosia.

20 Karson, J. A., et al. (1997), *Proc. ODP Scientific Results*, 153, Ocean Drilling Program,
21 College Station, TX.

22 Karson, J. A., et al. (2006), Detachment shear zone of the Atlantis Massif core complex,
23 Mid-Atlantic Ridge, 30°N, *Geochem. Geophys. Geosyst.*, 7, Q06016, doi:
24 10.1029/2005GC001109.

25 Kelemen, P. B., et al. (2007), Leg 209 summary: processes in a 20-km-thick conductive
26 boundary layer beneath the Mid-Atlantic Ridge, 14°–16°N. In Kelemen, P.B., Kikawa,
27 E., and Miller, D.J. (Eds.), *Proc. ODP, Sci. Results*, 209: College Station, TX (Ocean
28 Drilling Program), 1–33. doi:10.2973/odp.proc.sr.209.001.2007.

- 1 Kelley, D.S., et al. (2001), An off-axis hydrothermal vent field discovered near the Mid-
2 Atlantic Ridge at 30°N, *Nature*, *412*, 145-149.
- 3 Lagabriele, Y., et al. (1998), Ultramafic-mafic plutonic rock suites exposed along the
4 Mid-Atlantic Ridge (10°N-30°N): Symmetrical-asymmetrical distribution and
5 implications for seafloor spreading processes, in *Faulting and Magmatism at Mid-
6 Ocean Ridges*, edited by P. T. D. W.R. Buck, J.A. Karson, and Y. Lagabriele, pp.
7 153-176, American Geophysical Union, Washington, DC.
- 8 Lin, J., et al. (1990), Evidence from gravity data for focused magmatic accretion along
9 the Mid-Atlantic Ridge, *Nature*, *344*, 627-632. doi:10.1038/344627a0.
- 10 Lissenberg, C. J., and H. J. B. Dick (2008), Melt-rock reaction in the lower oceanic crust
11 and its implications for the genesis of mid-ocean ridge basalt, *Earth Planet. Sci. Lett.*,
12 *271*, 311-325. doi:10.1016/j.epsl.2008.04.023.
- 13 MacLeod, C. J., et al. (2002), Direct geological evidence for oceanic detachment faulting:
14 The Mid-Atlantic Ridge, *Geology*, *30*, 879-882. doi:10.1130/0091-7613(2002)
15 030<0879:DGEFOD>2.0.CO;2.
- 16 MacLeod, C. J., et al. (2009), Life cycle of oceanic core complexes, *Earth and Planetary
17 Science Letters*, *287*, 333-344, doi:10.1016/j.epsl.2009.08.016.
- 18 McCaig, A. M., et al. (2007), Oceanic detachment faults focus very large volumes of
19 black smoker fluids, *Geology*, *35*, 935-938, doi:10.1130/G23657A.1.
- 20 McCaig, A. M., et al. (2010), Detachment Fault Control on Hydrothermal Circulation
21 Systems: Interpreting the Subsurface Beneath the TAG Hydrothermal Field Using the
22 Isotopic and Geological Evolution of Oceanic Core Complexes in the Atlantic, in
23 *Diversity of Hydrothermal Systems on Slow Spreading Ocean Ridges*, P. Rona, et al.
24 (eds.), *Geophys. Mono.* 188, 207-240, AGU, Washington D.C.
- 25 Mehl, L. and G. Hirth (2008), Plagioclase preferred orientation in layered mylonites:
26 Evaluation of flow laws for the lower crust, *J. Geophys. Res.*, *113*, B05202, doi:
27 10.1029/2007JB005075.
- 28
29

- 1 Michibayashi, K., et al. (2008), Impermeable fault zone arising from high-T brittle shear
2 within in situ oceanic crust, 30°N Mid-Atlantic Ridge, *Earth Planet Sci. Lett.*, 275,
3 348-354, doi:10.1016/j.epsl.2008.08.033.
- 4 Minshull, T. A., et al. (1998), Is the oceanic Moho a serpentinization front?, in *Modern*
5 *ocean floor processes and the geological record*, edited, pp. 71-80, Geologic Society,
6 London. doi:10.1144/GSL.SP.1998.148.01.05.
- 7 Miranda, E. A., and Y. Dilek (2010), Oceanic Core Complex Development in Modern and
8 Ancient Oceanic Lithosphere: Gabbro-Localized versus Peridotite-Localized
9 Detachment Models, *J. Geol.*, 118, 95-109. doi:10.1086/648460.
- 10 Miranda, E. A., and B. E. John (2010), Strain localization along the Atlantis Bank oceanic
11 detachment fault system, Southwest Indian Ridge, *Geochem. Geophys. Geosyst.*, 11,
12 Q04002. doi:10.1029/2009GC002646
- 13 Morris, A., et al. (2009), Footwall rotation in an oceanic core complex quantified using
14 reoriented Integrated Ocean Drilling Program core samples, *Earth Planet. Sci. Lett.*,
15 287, 217-228, doi:10.1016/j.epsl.2009.08.007.
- 16 Nooner, S. L., et al. (2003), Constraints on crustal structure at the Mid-Atlantic Ridge
17 from seafloor gravity measurements made at the Atlantis Massif, *Geophys. Res. Lett.* ,
18 30, 1446-, doi:10.1029/2003GL017126.
- 19 Nozaka, T., et al. (2008), Formation of clay minerals and exhumation of lower-crustal
20 rocks at Atlantis Massif, Mid-Atlantic Ridge, *Geochem. Geophys. Geosys.*, 9, doi:
21 10.1029/2008GC002207.
- 22 Nozaka, T., and P. Fryer (2011), Alteration of the oceanic lower crust at a slow-spreading
23 axis: insight from vein-related zoned halos in olivine gabbro from Atlantis Massif, Mid-
24 Atlantic Ridge, accepted *J. Petrology* (in press) doi:10.1093/petrology/egq098.
- 25 Ohara, Y., et al. (2007), Seismic study on oceanic core complexes in the Parece Vela
26 back-arc basin, *Island Arc*, 16, 348-360, doi:10.1111/j.1440-1738.2007.00591.x.
- 27 OTTER (1984), The geology of the Oceanography transform: the ridge-transform
28 intersections, *Mar. Geophys. Res.*, 6, 109-141.
- 29

- 1 Pariso, J. E., et al. (1996), Three-dimensional inversion of marine magnetic anomalies:
2 implications for crustal accretion along the Mid-Atlantic Ridge (28°-31°30'N), *Mar.*
3 *Geophys. Res.*, *18*, 85-101.
- 4 Schouten, H., D.K. Smith, J.R. Cann, J. Escartín (2010) Tectonic versus magmatic
5 extension in the presence of core complexes at slow-spreading ridges from a
6 visualization of faulted seafloor topography, *Geology*, *38*, 615-618, doi:10.1130/
7 G30803.1.
- 8 Schroeder, T., and B. E. John (2004), Strain localization on an oceanic detachment fault
9 system, Atlantis Massif, 30°N, Mid-Atlantic Ridge, *Geochem., Geophys., Geosys.*, *5*,
10 Q11007, doi:10.1029/2004GC000728.
- 11 Schroeder, T., et al. (2007), Nonvolcanic seafloor spreading and corner-flow rotation
12 accommodated by extensional faulting at 15°N on the Mid-Atlantic Ridge: A structural
13 synthesis of ODP Leg 209, *Geochem. Geophys. Geosys.*, *8*(Q06015), doi:
14 10.1029/2006GC001567.
- 15 Singh, S. C., et al. (2004), New insights into serpentinization at Atlantis Massif, *Eos*
16 *Trans. AGU*, *85*(Fall Suppl.(47)), V23B-0628.
- 17 Sinton, J. M., and R. S. Detrick (1992), Mid-ocean ridge magma chambers, *J. Geophys.*
18 *Res.*, *97*, 197-216. doi:10.1029/91JB02508.
- 19 Smith, D.K., Escartín, J., Schouten, H. & Cann, J.R. (2008) Fault rotation and core
20 complex formation: significant processes in seafloor formation at slow-spreading Mid-
21 Ocean Ridges (Mid-Atlantic Ridge, 13 –15 N), *Geochem. Geophys. Geosyst.*, *9*,
22 Q03003, doi:10.1029/2007GC001699.
- 23 Suhr, G., et al. (2008), Stacked gabbro units and intervening mantle: a detailed look at a
24 section of IODP Leg 305, Hole 1309D, *Geochem. Geophys. Geosyst.*, *9*, doi:
25 10.1029/2008GC002012.
- 26 Tamura, A., et al. (2008), Petrology and geochemistry of peridotites from IODP Site
27 U1309 at Atlantis Massif, MAR 30°N: micro- and macro-scale melt penetrations into
28 peridotites, *Contrib. Mineral. Petrol.*, *155*, 491-509, doi:10.1007/s00410-007-0254-0.
- 29

- 1 Tucholke, B. E., and J. Lin (1994), A geological model for the structure of ridge segments
2 in slow spreading ocean crust *J. Geophys. Res.*, *99*, 11931-11958. doi:
3 10.1029/94JB00338
- 4 Tucholke, B. E., et al. (1998), Megamullions and mullion structure defining oceanic
5 metamorphic core complexes on the Mid-Atlantic ridge, *J. Geophys. Res.*, *103*,
6 9857-9866. doi:10.1029/98JB00167.
- 7 Tucholke, B. E., et al. (2008), Role of melt supply in oceanic detachment faulting and
8 formation of megamullions, *Geology*, *36*, 455–458, doi:10.1130/G24639A.1.
- 9 Von de Handt, A. and E. Hellebrand (2010) Transformation of mantle to lower crust:
10 melt-rock reaction processes in peridotites from Atlantis Massif, 30°N Mid-Atlantic
11 Ridge, Abstract V11A-2244 presented at 2010 Fall Mtg AGU, San Francisco, Calif.
12 13-17 Dec.
- 13 Wernicke, B., and G. J. Axen (1988), On the role of isostasy in the evolution of normal
14 fault systems, *Geology*, *16*, 848-851. doi:10.1130/0091-7613(1988)
15 016<0848:OTROII>2.3.CO;2.
- 16 White, R. S., et al. (1992), Oceanic crustal thickness from seismic measurements and rare
17 earth element inversions, *J. Geophys. Res.*, *97*, 19683-19715. doi:10.1029/92JB01749.
- 18 Xu, M., et al. (2009), Heterogeneous seismic velocity structure of the upper lithosphere at
19 Kane oceanic core complex, Mid-Atlantic Ridge, *Geochem. Geophys. Geosys.*, *10* (10),
20 Q10001,, doi:10.1029/2009GC002586.
- 21 Zhao, X., and M. Tominaga (2009), Paleomagnetic and rock magnetic results from lower
22 crustal rocks of IODP Site U1309: Implication for thermal and accretion history of the
23 Atlantis Massif, *Tectonophysics*, *474*, 435–448, doi:10.1016/j.tecto.2009.04.017.
- 24
25
26
27
28
29

Process	Constraint from Drilling Data
<i>subaxial magmatism</i>	
2-3 larger intrusions, total >1.4 km thick	different zircon dates (1.17/1.24 Ma) above/below ~600 mbsf downhole change in Mg# & Yb ~600-650 mbsf repeating pattern uphole, from less- to more-evolved rock type
many small (self) injections of melt	hundreds of individual petrologic units evolved rock type generally intrudes less evolved type
melt fluxes pre-existing olivine-rich rocks	troctolite olivine grains not in equilibrium w/ interstitial plagioclase all (sparse) peridotites have later melt crystallized within them
crystallization of main intrusions	1230 °C, < 200 MPa
<i>alteration and strain localization</i>	
minor shearing at higher temperature	brown hornblende, clinopyroxene, orthopyroxene, olivine, plagioclase all stable in thin mylonites; T> 800 °C; rapid cooling through this interval
static hydration and cataclasis mainly in a progressively cooling regime, some fluctuations	wide range amphibole compositions: green hornblende-actinolite replacing pyroxene; tremolite-chlorite corona replace olivine & plagioclase; Locally, hornblende overprints tremolite in coronas & talc+tremolite replaces serpentine (up-T reactions). T 750-400 °C
detachment formation	poorly sampled talc-tremolite schist with ultramafic protolith, same properties as seafloor detachments mapped elsewhere. Amphibole-rich breccia/cataclastic zones cut by basalt/diabase intrusions suggest detachment faulting in gabbro and diabase
uplift, flexure, exposure of detachment fault; rapid cooling to ambient gradient (~100 °C/km)	Corona reactions replaced by serpentine (antigorite, then lizardite + brucite, then lizardite plus magnetite) and microrodingites at 200-350 °C. Late clay-filled veins concentrated in lower part of core. Zeolites only found deeper than 700 mbsf. Palaeomagnetic rotations of 45° since cooling below Curie Point
<i>continued exhumation</i>	
weathering, sedimentation of fault at seafloor	talc-tremolite schist fragments, fossiliferous deposits and hyaloclastic debris
low-T alteration	alteration of halos surrounding leucocratic veins, clay veining lizardite veins in serpentinized olivine-rich troctolite ~1090 mbsf

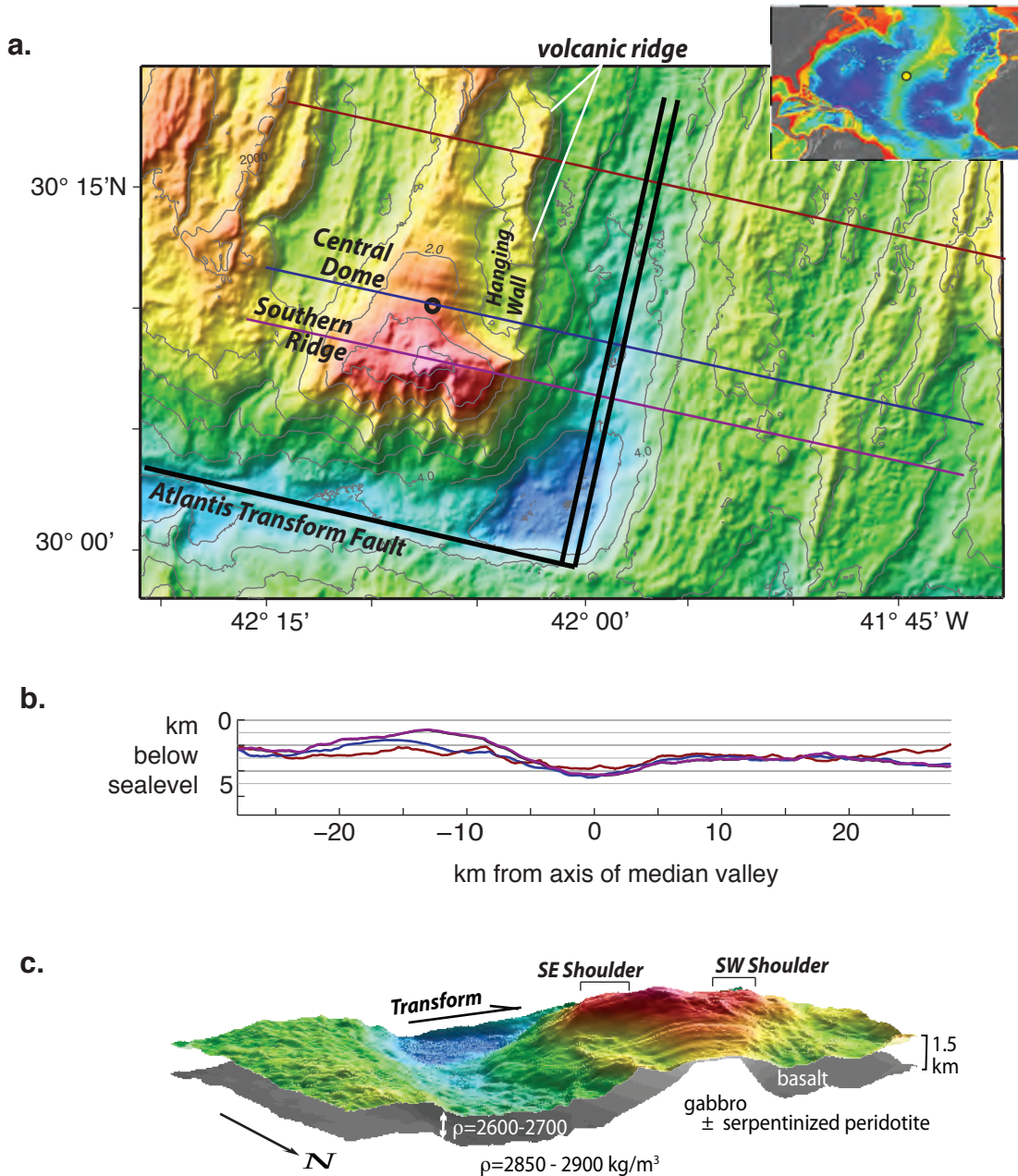


Figure 1. Seafloor topography in the vicinity of the intersection of the Mid-Atlantic Ridge and Atlantis transform fault and basic structure of Atlantis Massif oceanic core complex. a) Contour interval 0.5 km. Corrugated surface is inferred to be exposed detachment capping the domal high. Axis of the Mid-Atlantic Ridge and Atlantis Transform Fault are shown by black lines; circle marks IODP Site U1309. Location of profiles across the middle of the segment (brown), the Central Dome (blue) and the Southern Ridge (purple) is shown. b) Seafloor depth along these 3 profiles. c) Perspective view of Atlantis Massif looking SSW. Gray interface shows 3-D model of upper/lower crustal boundary that can explain most of the Bouguer gravity anomaly in this area.

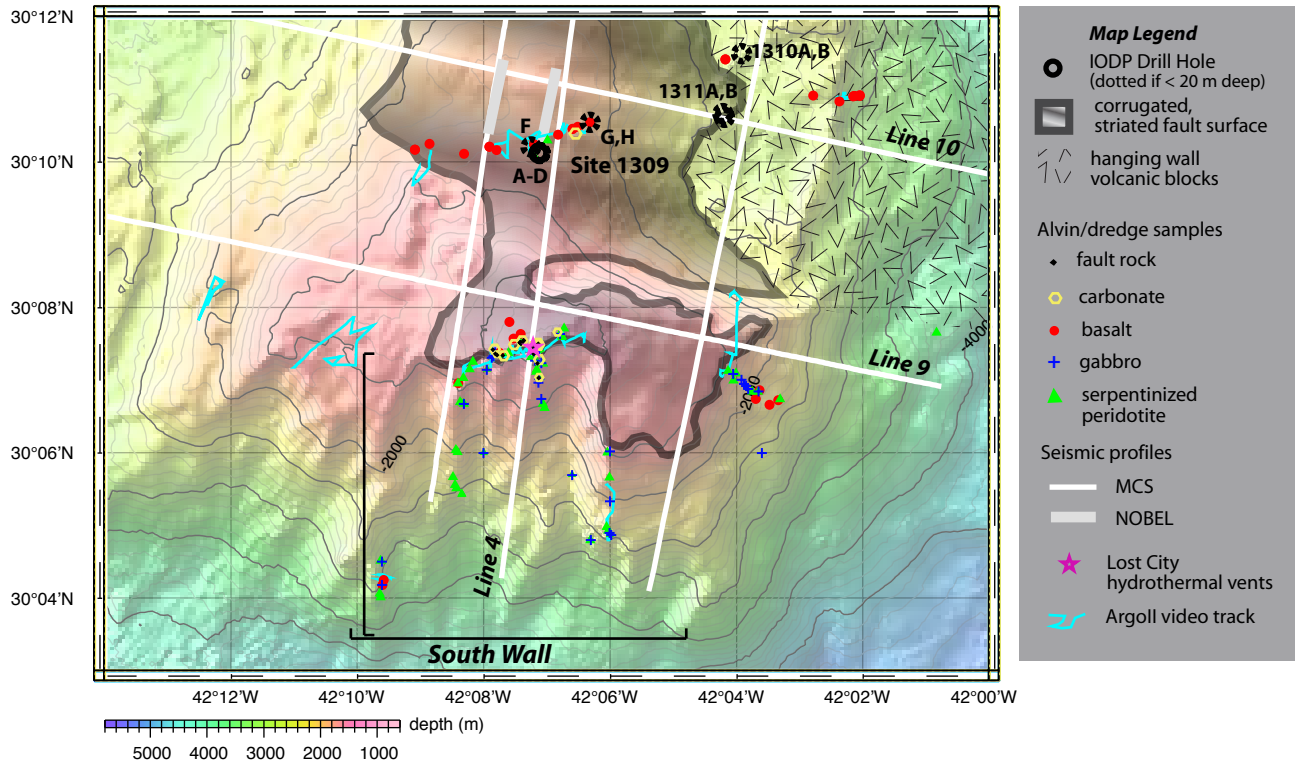


Figure 2. Geologic data and selected geophysical tracks at Atlantis Massif. Sonar coverage is complete at 100-m scale as is sidescan at 10-m scale. The latter delineates extent of striations that parallel corrugations on the exposed detachment fault that caps the domal core comprising the footwall of the OCC. The volcanic hanging wall juxtaposed east of the Central Dome flanks the median valley of the spreading axis. Majority of rock sample symbols indicate collection by submersible, as indicated by close spacing along relatively continuous paths. MCS— multichannel seismic line; NOBEL— near bottom seismic source shooting line with seafloor seismographs located at each end.

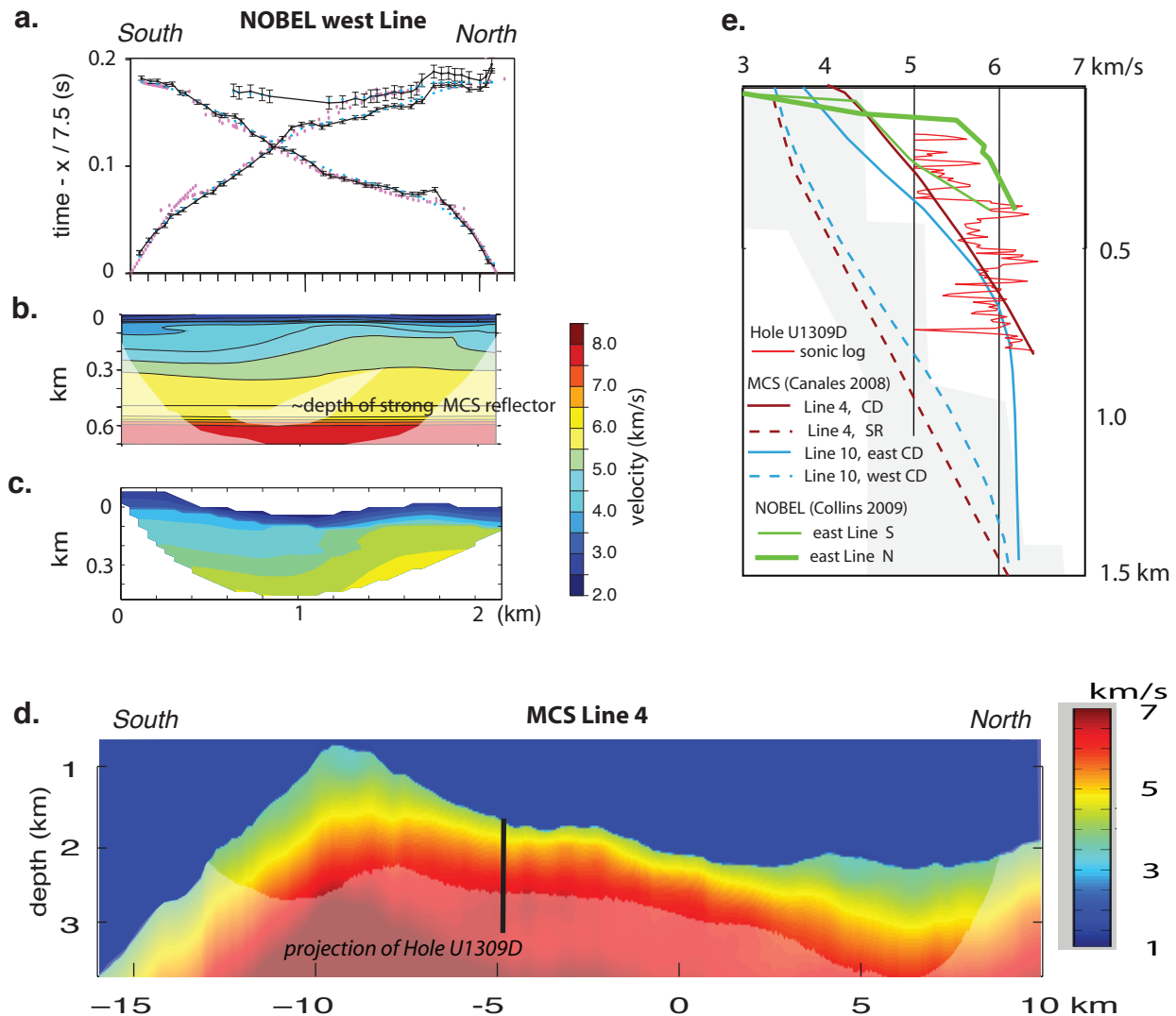


Figure 3. Seismic refraction results. a-c) western NOBEL line on the Central Dome (location in Figure 2): a) travel-time picks (black) and predicted travel times—cyan for model in b; pink for model in c. b) Velocity model based on inversion of Collins et al. (2003). Areas with no ray coverage are semi-opaque. c) Preferred velocity model determined from forward modeling by Collins et al. (2009). Seafloor topography is included here, unlike in b. While this travel-time effect, alone, does not preclude the presence of >7.5 km/s layer, other data do rule one out at shallow depths. d) Velocity model based on inversion of MCS refractions for Line 4 by Canales et al. (2008). Both color scale and vertical exaggeration differ from that used for b & c. Area in d not constrained by raypaths is semi-opaque. e) Selected velocity depth profiles illustrate variability within/between structural blocks; light gray region indicates range of typical young Atlantic crustal profiles (White et al., 1992).

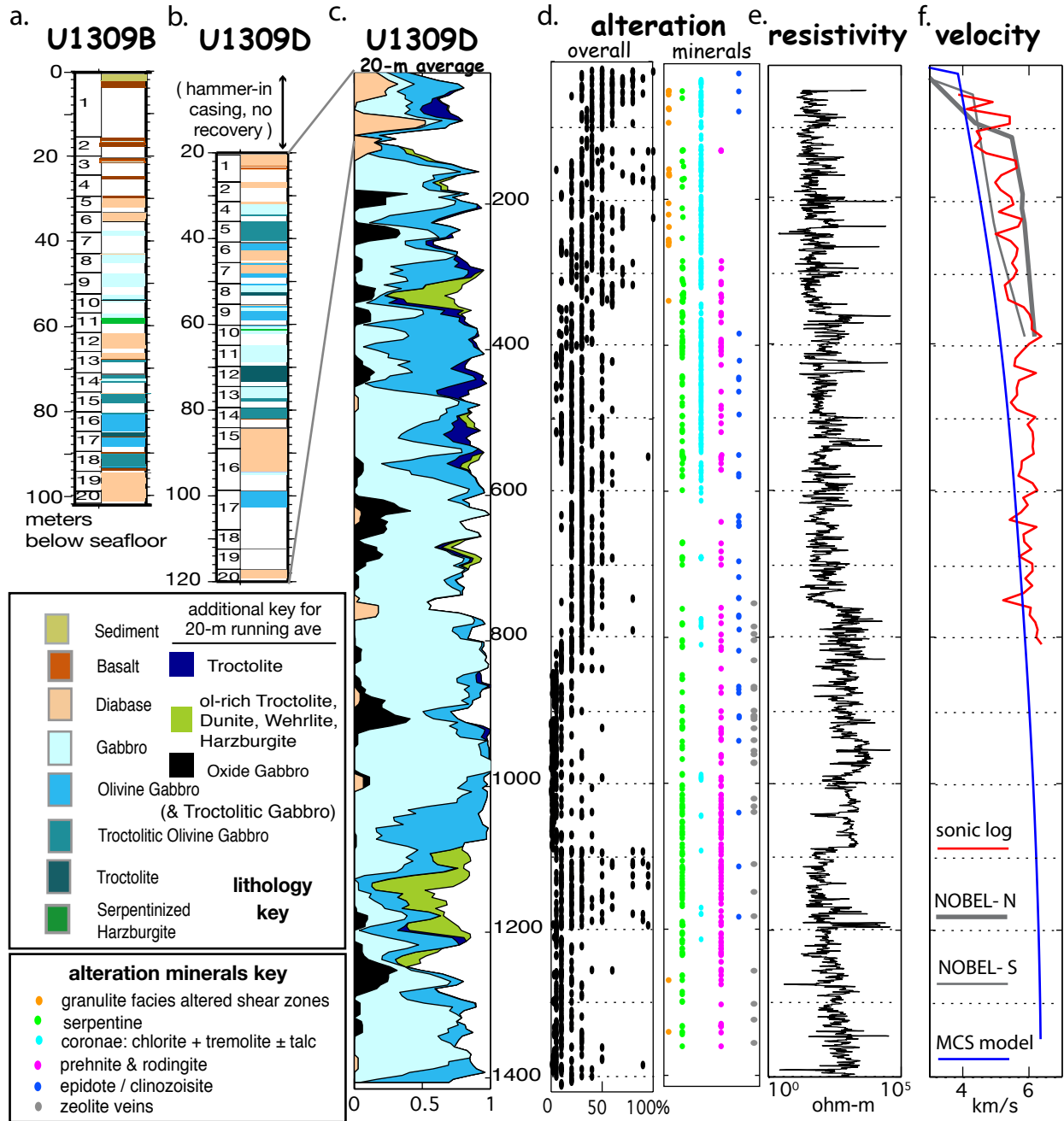


Figure 4. Downhole results at IODP Site U1309. a) Hole U1309B lithology. b) Hole U1309D lithology in uppermost section. c) Hole U1309D lithology with 20-m running average over individual igneous units; white shows fraction of corresponding section that was not recovered. d) Overall alteration and corona occurrence, from shipboard visual core description, and presence of selected alteration minerals, from thin section log (amount of minerals not shown). e) Dual-laterolog recording of deep resistivity of wallrock in Hole U1309D. f) Seismic compressional wave velocity. Logged value in Hole U1309D shown by red curve. Profiles extracted from nearby refraction velocity models are also shown (NOBEL- Collins et al., 2009; MCS portion of Line 10- Blackman et al., 2009).

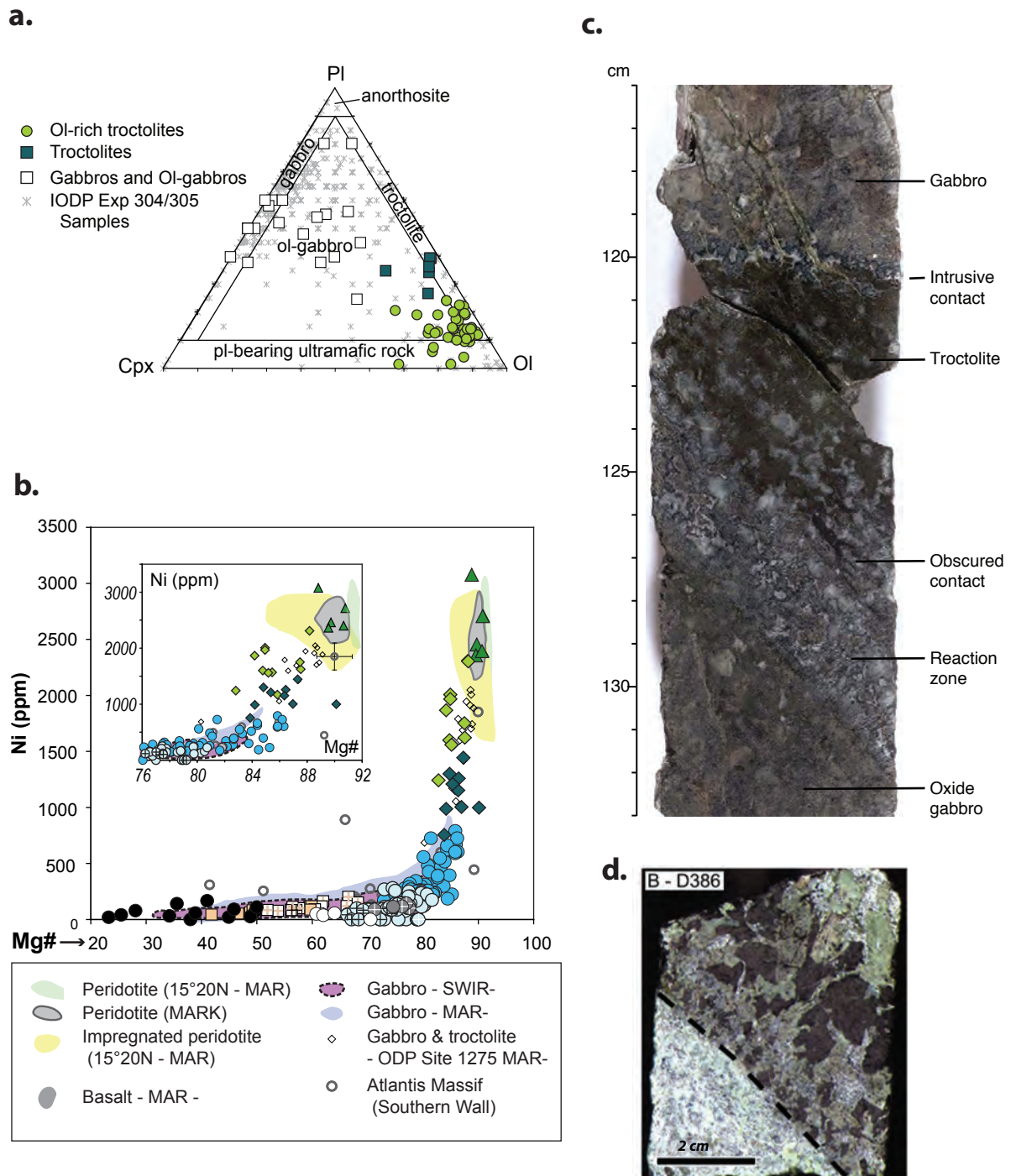


Figure 5. Petrology, geochemistry, and photographs of Site U1309 core samples. a) Compositions for representative suite of samples from the site are shown by small gray symbols. Other symbols indicate samples from within the intervals that are dominantly olivine-rich troctolite that were studied in detail by Drouin *et al.* (2009). b) Bulk rock chemistry for Site U1309 (symbol color key same as Fig. 4) and comparison with other areas (shaded fields). (from Godard *et al.*, 2009). c) Photo of Core 304-U1309D-69R-1 shows intrusive contact between gabbro and troctolite and lower contact that is a reaction zone between the troctolite and a later oxide gabbro injection. d) Oxide gabbro dike intrudes gabbro (upper unit) with a sharp lower contact with gabbro (from Grimes *et al.*, 2008)

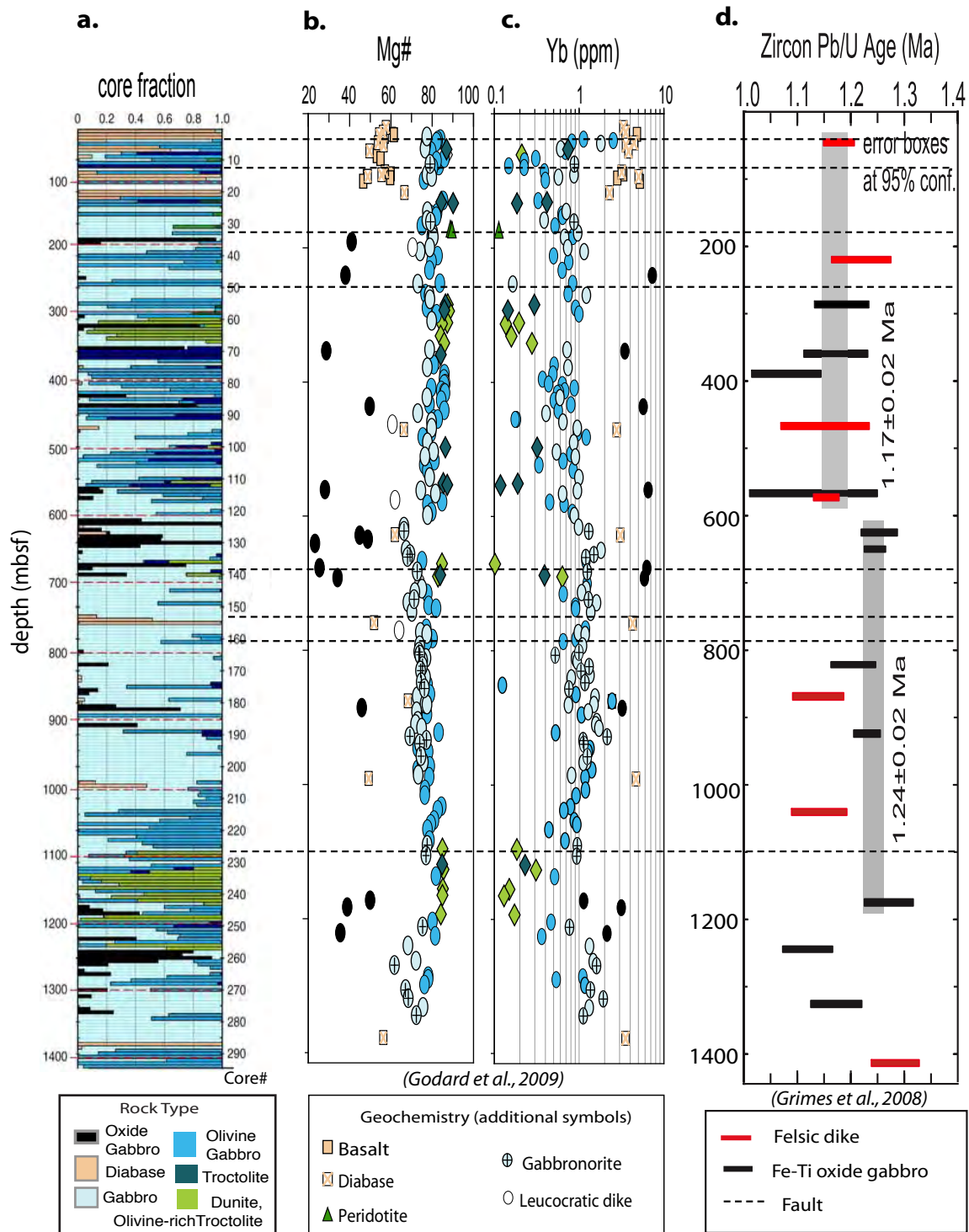


Figure 6. Downhole igneous variation in Hole U1309D. a) Proportion of rock type recovered in each core section (core number on right side of column). b) Bulk rock magnesium number $MgO/(MgO+FeO)$. c) Bulk rock trace element measurements for Ytterbium. d) Age dates obtained for core samples. Horizontal dashed lines indicate fault zones inferred from cataclastic deformation or fault gouge in core and (below 35mbsf) coinciding wall rock structure observed in images (resistivity) or porosity.

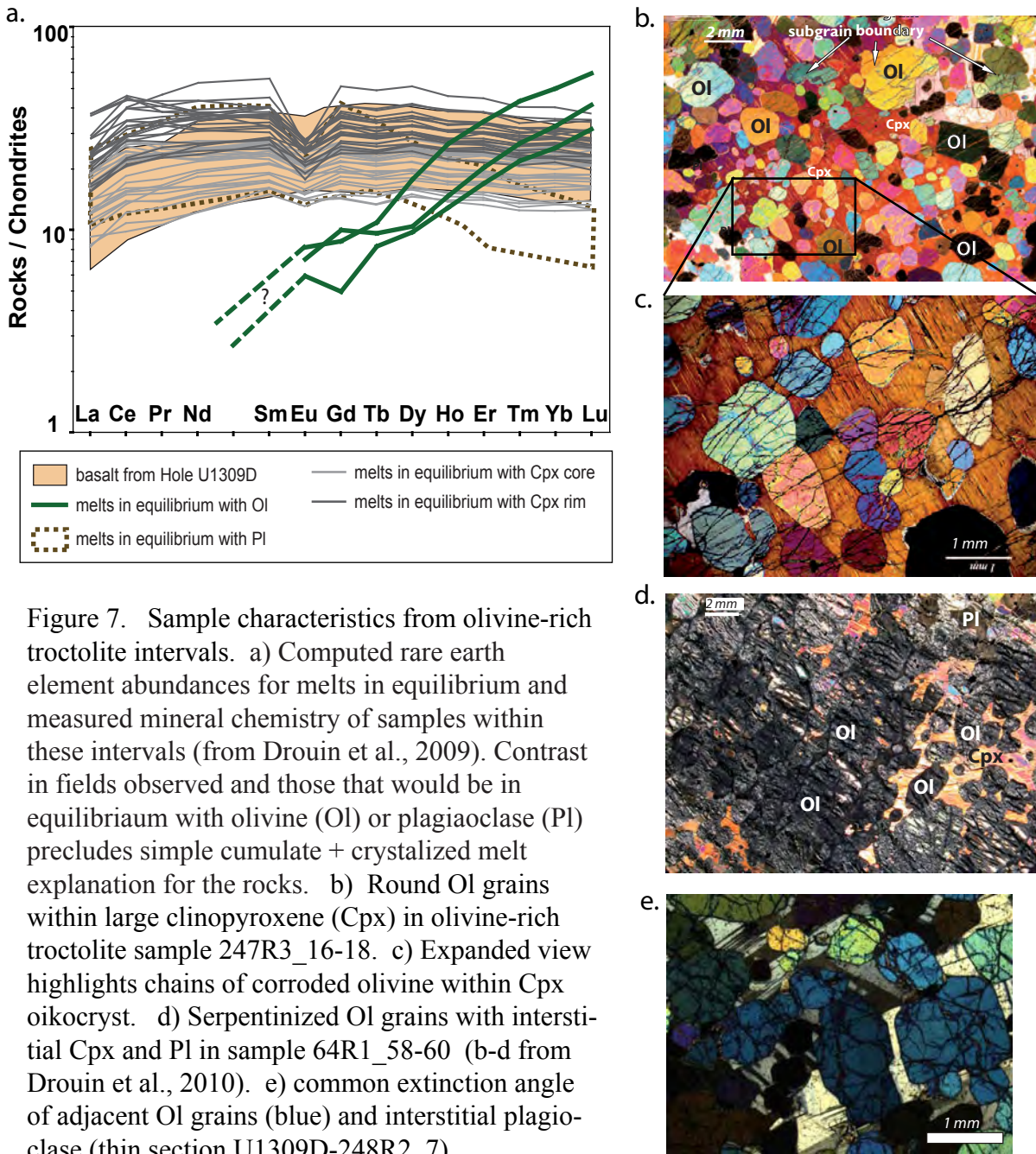


Figure 7. Sample characteristics from olivine-rich troctolite intervals. a) Computed rare earth element abundances for melts in equilibrium and measured mineral chemistry of samples within these intervals (from Drouin et al., 2009). Contrast in fields observed and those that would be in equilibrium with olivine (Ol) or plagioclase (Pl) precludes simple cumulate + crystalized melt explanation for the rocks. b) Round Ol grains within large clinopyroxene (Cpx) in olivine-rich troctolite sample 247R3_16-18. c) Expanded view highlights chains of corroded olivine within Cpx oikocryst. d) Serpentinized Ol grains with interstitial Cpx and Pl in sample 64R1_58-60 (b-d from Drouin et al., 2010). e) common extinction angle of adjacent Ol grains (blue) and interstitial plagioclase (thin section U1309D-248R2_7).

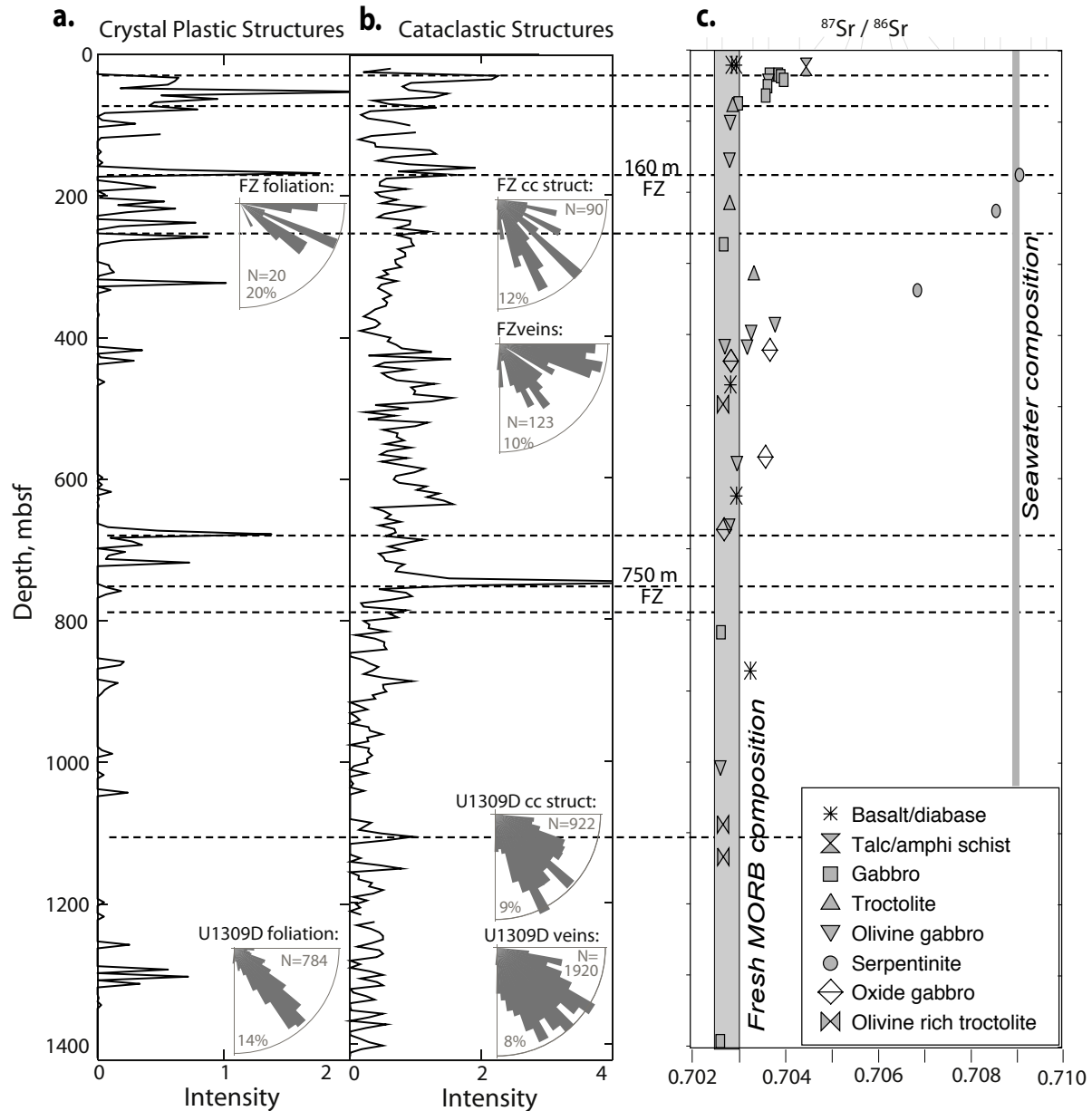


Figure 8. Downhole deformation in core from Hole U1309D (Hirose and Hayman, 2008) and evidence of extent of seawater penetration into the formation. a) Intensity of crystal plastic deformation along core sections on scale of 0-5 (low-high). b) Intensity of cataclastic deformation along core sections on scale 0-5. Rose diagrams in a & b show orientation with respect to downhole direction, no correction for paleomagnetically deduced footwall rotation indicated. Upper diagrams refer only to structures measured within the fault zone ~160 mbsf; lower diagrams are for entire hole. c) Strontium isotope ratios measured on selected core samples with comparison to values for fresh MORB and seawater (McCaig et al., 2010). Dashed lines indicate fault zones identified on the basis of core and borehole logging information.

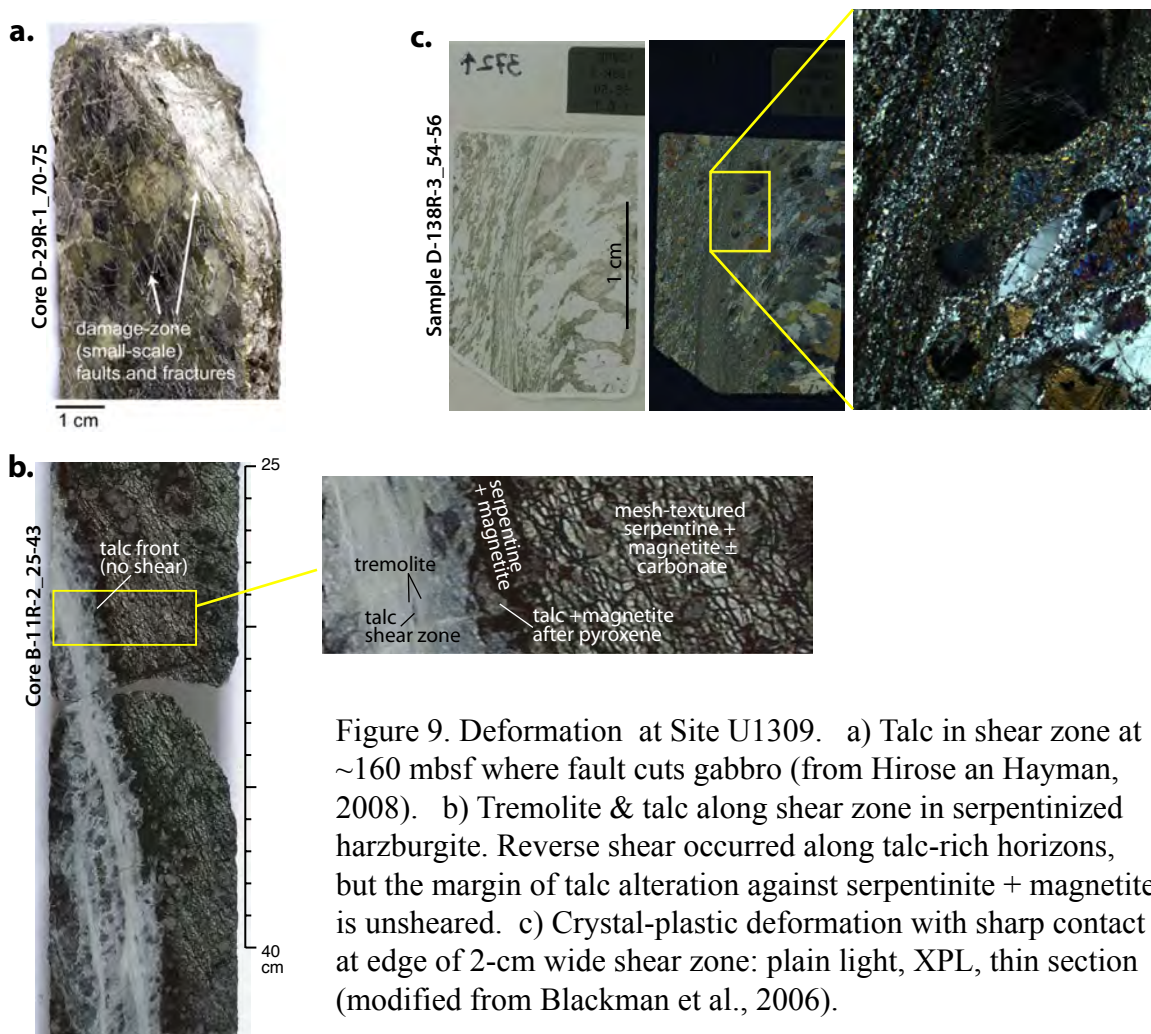


Figure 9. Deformation at Site U1309. a) Talc in shear zone at ~160 mbsf where fault cuts gabbro (from Hirose and Hayman, 2008). b) Tremolite & talc along shear zone in serpentized harzburgite. Reverse shear occurred along talc-rich horizons, but the margin of talc alteration against serpentinite + magnetite is unsheared. c) Crystal-plastic deformation with sharp contact at edge of 2-cm wide shear zone: plain light, XPL, thin section (modified from Blackman et al., 2006).

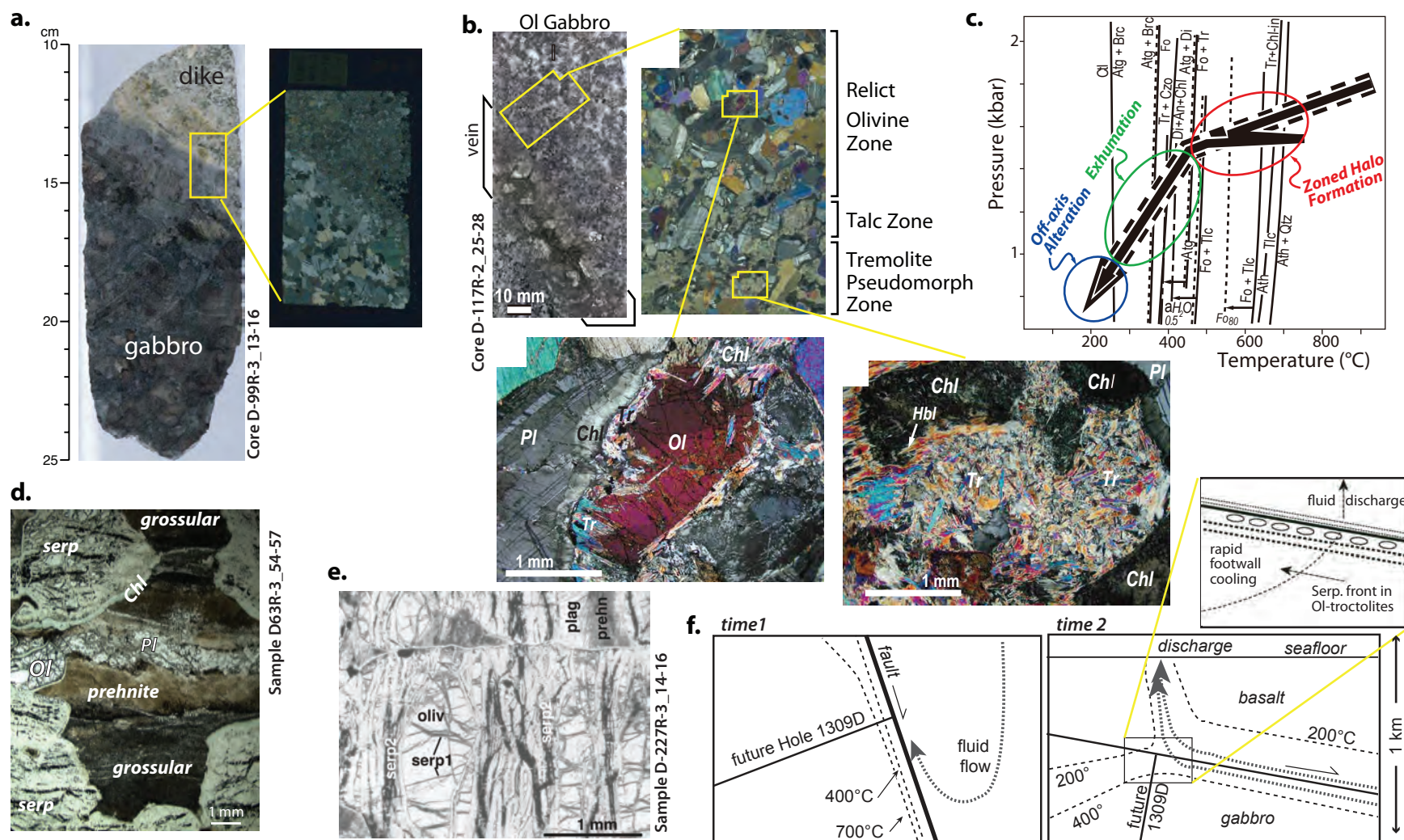


Figure 10. Alteration at Site U1309. a) Alteration front where leucocratic dike intruded gabbro (modified from Blackman et al., 2006). b) Zoned halo surrounding leucocratic vein; tremolite pseudomorph zone is closest to vein. c) P-T history of core >350 mbsf (b & c modified from Nozaka & Fryer, 2011) d) Olivine-rich troctolite thin section shows prehnite-grossular-chlorite assemblage associated with serpentinization (after Frost et al. 2008). e) Two stages of veins in 50-70% serpentinized sample (from Beard et al., 2009). f) Thermal history of the detachment footwall interpreted in terms of cooling by hydrothermal fluid flow up the fault and episode(s) of fluid discharge to seafloor that impact gradient (based on McCaig et al., 2010, where fault & fluid flow patterns are inferred on basis of seismicity and venting, respectively, at TAG hydrothermal field).

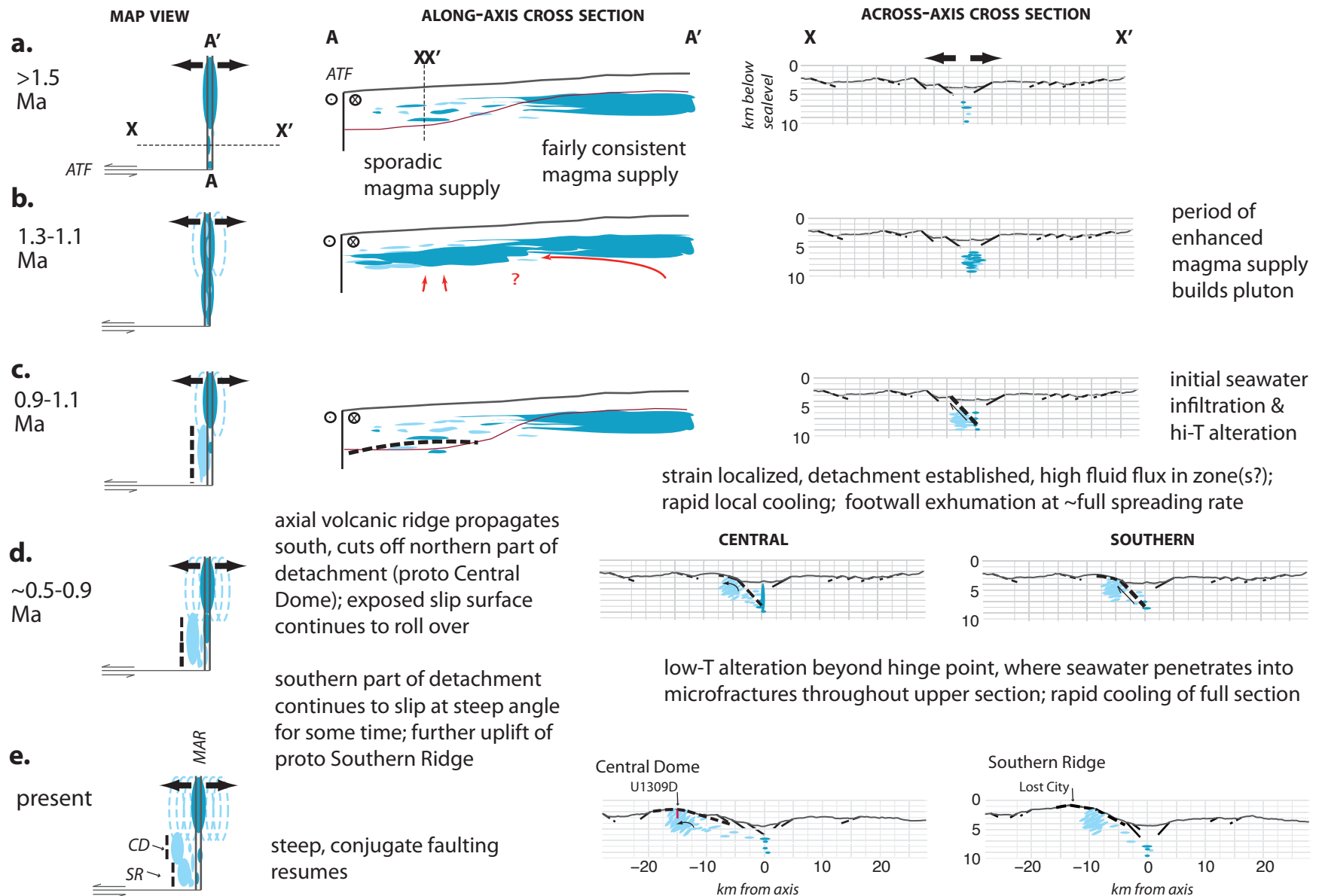


Figure 11. Working model for 3-D evolution of Atlantis Massif OCC. Thick dash shows active fault, thin dash shows inactive trace (in map view, line thickness relates to activity below seafloor, to east of surface trace shown). Dark blue indicates current magmatism; light blue indicates past intrusion.